IEEE Access
Multidisciplinary | Rapid Review | Open Access Journal

Received October 23, 2016, accepted December 1, 2016, date of publication December 7, 2016, date of current version January 27, 2017.

Digital Object Identifier 10.1109/ACCESS.2016.2636159

Fractional-Order Euler-Lagrange Equation for Fractional-Order Variational Method: A Necessary Condition for Fractional-Order Fixed Boundary Optimization Problems in Signal Processing and Image Processing

YI-FEI PU
College of Computer Science, Sichuan University, Chengdu 610065, China (puyifei_007@hotmail.com)

This work was supported in part by the Foundation Franco-Chinoise Pour La Science Et Ses Applications, in part by the National Natural Science Foundation of China under Grant 61571312, in part by the Science and Technology Support Project of Sichuan Province of China under Grant 2013SZ0071, and in part by the Science and Technology Support Project of Chengdu PU Chip Science and Technology Company, Ltd.

ABSTRACT This paper discusses a novel conceptual formulation of the fractional-order Euler–Lagrange equation for the fractional-order variational method, which is based on the fractional-order extremum method. In particular, the reverse incremental optimal search of the fractional-order variational method is based on the fractional-order steepest descent approach. Fractional calculus has been applied to the solution of a necessary condition for the fractional-order fixed boundary optimization problems in signal processing and image processing mainly because of its inherent strengths in terms of long-term memory, non-locality, and weak singularity. At first, for the convenience of comparison, the first-order Euler–Lagrange equation for the first-order variational method is derived based on the first-order Green formula. Second, the fractional-order Euler–Lagrange equation for the fractional-order variational method is derived based on Wiener–Khintchine theorem. Third, in order to directly and easily achieve the fractional-order variational method in the spatial domain or the time domain, the fractional-order Green formula and the fractional-order Euler–Lagrange equation based on the fractional-order Green formula are derived, respectively. Fourth, the solution procedure of the fractional-order Euler–Lagrange equation is derived. Finally, a fractional-order inpainting algorithm and a fractional-order denoising algorithm based on the fractional-order variational method are illustrated, respectively. The capability of restoring and maintaining the edges and textural details of the fractional-order image restoration algorithm based on the fractional-order variational method is superior to that of the integer-order image restoration algorithm based on the classical first-order variational method, especially for images rich in textural details. The fractional-order Euler–Lagrange equation for the fractional-order variational method proposed by this paper is a necessary condition for the fractional-order fixed boundary optimization problems, which is a basic mathematical method in the fractional-order optimization and can be widely applied to the fractional-order field of signal analysis, signal processing, image processing, machine intelligence, automatic control, biomedical engineering, intelligent transportation, computational finance and so on.

INDEX TERMS Fractional calculus, fractional-order Green formula, fractional-order steepest descent approach, fractional-order extreme point, fractional-order image restoration.

I. INTRODUCTION

It is well known that variational method is an important part of functional analysis, which was firstly introduced by Euler in 1744 [1], [2]. In 1755, Joseph-Louis Lagrange proposed a revolutionary technique of variations in his brief letter written to Euler [3]. The classical cases of the integer-order

variational method include Fermat's principle of least time, Bernoulli's brachistochrone problem [4], and the isoperimetric problem. Variational method allows us to solve optimization problems using only elementary calculus [5], [6]. The key point of variational method is to determine the function that achieves the extremum seeking algorithm of a functional. The classical first-order Euler-Lagrange equation can be obtained by setting the first-order derivatives of the corresponding functional with regard to each parameter be equal to zero [5], [6]. In addition, the Rayleigh-Ritz method and Galerkin's method led to the formulation of the finite element method for implementing the prediction of a physical process [7], [8]. Because many ordinary and partial differential equations in mathematics, physics, and engineering can be derived as the first-order Euler equation for an appropriate corresponding functional, the integer-order variational method is now widely applied to many scientific fields such as numerical analysis [9], nonconvex problems [10], mechanics [5], [11], chemistry [12], [13], scattering problems [14], electromagnetic field problems [15], control [16], signal processing and image processing [17]–[29], and so on.

Nowadays, fractional calculus has been developed as an important branch of mathematical analyses [30]–[34], which is as old as the integer-order calculus. Fractional calculus extends the concepts of the integer-order difference and Riemann sums. Although until recently, the applications of fractional calculus mainly focused concentration on the field of mathematics and now seem to be a promising mathematical approach for the physical scientists and engineering technicians. More and more scientific researches show that a fractional-order or a fractional dimensional method is now one of the best way to describe many natural phenomena such as the fractional diffusion processes [35]–[37], fractional viscoelasticity theory [38], fractal dynamics [39], fractional control [40], [41], fractional neural networks [42]–[47], fractional signal processing [48]–[62], and fractional image processing [63]–[75], and many other fields in physics [76]–[99].

How to apply fractional calculus to variational method is an emerging scientific field that has been seldom received desired attention. With regard to a signal, the features of its fractional calculus are quite different from those of its integer-order calculus. For example, the fractional differential, except based on the Caputo definition, of a Heaviside function is equal to non-zero, whereas its integer-order differential must be equal to zero [30]–[34]. Fractional calculus has been successfully applied to signal processing and image processing mainly because of its inherent strengths in terms of long-term memory, non-locality, and weak singularity [48]–[75]. For instance, fractional calculus was firstly introduced to image processing by Pu in 2006 [62], [63]. A fractional differential mask can nonlinearly maintain the low-frequency contour features in the smooth area of an image and enhance the high-frequency edges and textural details in those areas where the grey level undergoes frequent or unusual variations [62]–[69]. Therefore, to solve a necessary condition for the fractional-order fixed boundary optimization problems in signal processing and image processing, an interesting theoretical problem emerges naturally: what the fractional-order Euler-Lagrange equation for the fractional-order variational method is. Motivated by this need, in this paper, we introduce a novel conceptual formulation of the fractional-order Euler-Lagrange equation for the fractional-order variational method, which is based on the fractional-order extremum method. In particular, the reverse incremental optimal search of the fractional-order variational method is based on the fractional-order steepest descent approach [73].

The rest of the manuscript is organized as follows: Section 2 presents in brief the necessary mathematical background of fractional calculus. Section 3 proposes the formulation of the fractional-order Euler-Lagrange equation for the fractional-order variational method. At first, for the convenience of comparison, the first-order Euler-Lagrange equation for the first-order variational method is derived based on the first-order Green formula. Secondly, the fractional-order Euler-Lagrange equation for the fractional-order variational method is derived based on Wiener-Khintchine theorem. Thirdly, in order to directly and easily achieve the fractional-order variational method in spatial domain or time domain, the fractional-order Green formula and the fractional-order Euler-Lagrange equation based on the fractional-order Green formula are derived, respectively. Fourthly, the solution procedure of the fractional-order Euler-Lagrange equation is derived. Section 4 presents the experiment results obtained and the associated analyses carried out. Here, first, a fractional-order inpainting algorithm based on the fractional-order variational method is illustrated. Second, a fractional-order denoising algorithm based on the fractional-order variational method is illustrated. In Section 5, the conclusions of this manuscript are presented.

II. MATHEMATICAL BACKGROUND

This section presents a brief introduction to the necessary mathematical background of fractional calculus.

The commonly used fractional calculus definitions in the domain of Euclidean measure are those of Grünwald-Letnikov, Riemann-Liouville, and Caputo [30]–[34]. In addition, there are some other well-known definitions of fractional derivative [100]–[112]. The Grünwald-Letnikov definition of fractional calculus, in a convenient form, for causal signal $f(x)$, is as follows:

$$
\begin{aligned}
&{}_{a}^{G-L}D_{x}^{v}f(x) \\
&= \lim_{N\to\infty}\left\{\frac{\left(\frac{x-a}{N}\right)^{-v}}{\Gamma(-v)}\sum_{k=0}^{N-1}\frac{\Gamma(k-v)}{\Gamma(k+1)}f\left(x-k\left(\frac{x-a}{N}\right)\right)\right\},
\end{aligned}
\tag{1}
$$

where $f(x)$ is a differintegrable function [30]–[34], $[a, x]$ is the duration of $f(x)$, v is a real number, $\Gamma(\alpha) = \int_0^\infty e^{-x}x^{\alpha-1}dx$

is the Gamma function, and ${}_{a}^{G-L}D_{x}^{v}$ denotes the Grünwald-Letnikov defined fractional differential operator.

The Riemann-Liouville definition of the v-order integral, for causal signal $f(x)$, is as follows:

$$ {}_{a}^{R-L}I_{x}^{v}f(x) = \frac{1}{\Gamma(v)}\int_{a}^{x}\frac{f(\tau)}{(x-\tau)^{1-v}}d\tau, \tag{2}$$

where $v > 0$ and ${}_{a}^{R-L}I_{x}^{v}$ denotes the Riemann-Liouville left-sided fractional integral operator. The Riemann-Liouville definition of the v-order derivative is as follows:

$$ {}_{a}^{R-L}D_{x}^{v}f(x) = \frac{1}{\Gamma(n-v)}\frac{d^{n}}{dx^{n}}\int_{a}^{x}\frac{f(\tau)}{(x-\tau)^{v-n+1}}d\tau, \tag{3}$$

where $n-1 \le v < n$, and ${}_{a}^{R-L}D_{x}^{v}$ denotes the Riemann-Liouville left-handed fractional differential operator. The Laplace transform of the v-order Riemann-Liouville differential operator [113]–[115] are given as:

$$\begin{aligned} FT[{}_{0}^{R-L}D_{x}^{v}f(x)] &= (\mathrm{j}\omega)^{v}\,FT[f(x)] \\ &\quad - \sum_{k=0}^{n-1}(\mathrm{j}\omega)^{k}\left[{}_{0}^{R-L}D_{x}^{v-1-k}f(x)\right]_{x=0}, \end{aligned} \tag{4}$$

$$\begin{aligned} LT[{}_{0}^{R-L}D_{x}^{v}f(x)] &= s^{v}LT[f(x)] \\ &\quad - \sum_{k=0}^{n-1}s^{k}\left[{}_{0}^{R-L}D_{x}^{v-1-k}f(x)\right]_{x=0}, \end{aligned} \tag{5}$$

where $FT()$ denotes Fourier transform, $LT()$ denotes Laplace transform, j denotes an imaginary unit, ω denotes an angular frequency, and $s = \mathrm{j}\omega$ denotes a Laplace operator. When $f(x)$ is a causal signal, and its fractional primitives are also required to be zero, we can simplify the Laplace transform for ${}_{0}^{R-L}D_{x}^{v}f(x)$ as, respectively:

$$FT[{}_{0}^{R-L}D_{x}^{v}f(x)] = (\mathrm{j}\omega)^{v}\,FT[f(x)], \tag{6}$$

$$LT[{}_{0}^{R-L}D_{x}^{v}f(x)] = s^{v}LT[f(x)]. \tag{7}$$

If signal $f(x)$ is a $(m+1)$-order continuously differentiable function, and $m = [v] = n-1$, where $[v]$ is the round-off number of v, the Grünwald-Letnikov defined fractional calculus is equivalent to the Riemann-Liouville defined one. If the aforementioned condition is not satisfied, the Riemann-Liouville defined fractional calculus is the extension of the Grünwald-Letnikov defined one. Thus, the Riemann-Liouville defined fractional calculus is with more extensive application potential. In this work, we mainly adopt the Riemann-Liouville defined fractional calculus for the following mathematical derivation. We use the equivalent notations $D_{\mathrm{x}}^{v} = {}_{0}^{G-L}D_{x}^{v} = {}_{0}^{R-L}D_{x}^{v}$ in an arbitrary, interchangeable manner.

III. FRACTIONAL-ORDER EULER-LAGRANGE EQUATION FOR FRACTIONAL-ORDER VARIATIONAL METHOD

In this section, with respect to a necessary condition of the fractional-order fixed boundary optimization problems in signal processing and image processing, two different equivalent forms of the fractional-order Euler-Lagrange equation for the fractional-order variational method are derived based on Wiener-Khintchine theorem and the fractional-order Green formula, respectively. For the convenience of illustration, without loss of generality, two-dimensional related issues are only discussed in this section. Likewise, the results of multi-dimensional issues are similar to those of two-dimensional issues.

A. FIRST-ORDER EULER-LAGRANGE EQUATION BASED ON FRACTIONAL-ORDER GREEN FORMULA

In this subsection, for the convenience of comparison, based on the first-order Green formula, the first-order Euler-Lagrange equation for the first-order variational method [6], [16], [17] need be derived.

Lemma 1: With regard to a first-order continuously differentiable scalar function $u(x,y)$ and a first-order continuously differentiable vector function $\vec{\boldsymbol{\varphi}} = (\varphi_x, \varphi_y)$, based on the first-order Green formula, an identical equation for the first-order variational method can be derived as:

$$\begin{aligned} \iint_{\Omega} u\,div\vec{\boldsymbol{\varphi}}\,dxdy &= \iint_{\Omega} u\,(\nabla \bullet \vec{\boldsymbol{\varphi}})\,dxdy \\ &= -\iint_{\Omega}\nabla u \bullet \vec{\boldsymbol{\varphi}}\,dxdy \\ &= -\langle \nabla u, \vec{\boldsymbol{\varphi}}\rangle \\ &= -\left\langle u, \nabla^{*}\vec{\boldsymbol{\varphi}}\right\rangle \\ &= \iint_{\Omega} u\left(-\nabla^{*}\vec{\boldsymbol{\varphi}}\right)dxdy, \end{aligned} \tag{8}$$

where $u(x,y)$ is an admissible surface (a test function), Ω is an open bounded subsets of real plane R^2 with smooth boundary, Ω bears a rectangular shape for most real applications, div denotes the first-order divergence operator, $dxdy$ is the Lebesgue measure on real plane R^2, symbol $\bullet$ denotes the first-order Euclidean inner product, symbol $\langle,\rangle$ denotes the first-order Euclidean inner product, and ∇^{*} denotes the first-order Hilbert adjoint operator [116] of a Hamilton operator ∇. Note that $\frac{\partial\varphi_x}{\partial x} + \frac{\partial\varphi_y}{\partial y} = 0$ is the first-order Euler-Lagrange equation of $-\iint_{\Omega}\nabla u \bullet \vec{\boldsymbol{\varphi}}\,dxdy = 0$.

Proof: A Hamiltonian can be defined by:

$$\begin{aligned} \nabla u &= \left(\frac{\partial}{\partial x}, \frac{\partial}{\partial y}\right)u \\ &= \left(\frac{\partial u}{\partial x}, \frac{\partial u}{\partial y}\right), \end{aligned} \tag{9}$$

where $u = u(x,y) \in C_0^1(\Omega)$ denotes a scalar function. Thus, from (9), the following can be obtained, respectively:

$$\begin{aligned} \nabla u \bullet \vec{\boldsymbol{\varphi}} &= \left(\frac{\partial u}{\partial x}, \frac{\partial u}{\partial y}\right) \bullet (\varphi_x, \varphi_y) \\ &= \frac{\partial u}{\partial x}\varphi_x + \frac{\partial u}{\partial y}\varphi_y, \end{aligned} \tag{10}$$

$$\begin{aligned} div\vec{\varphi} &= \frac{\partial \varphi_x}{\partial x} + \frac{\partial \varphi_y}{\partial y} \\ &= \left(\frac{\partial}{\partial x}, \frac{\partial}{\partial y}\right) \bullet (\varphi_x, \varphi_y) \\ &= \nabla \bullet \vec{\varphi}, \end{aligned} \tag{11}$$

where $\vec{\varphi} = (\varphi_x, \varphi_y)$ denotes a vector function, and div denotes the first-order divergence operator. Thus, from (11), one can obtain:

$$udiv\vec{\varphi} = u\frac{\partial \varphi_x}{\partial x} + u\frac{\partial \varphi_y}{\partial y}. \tag{12}$$

Thus, from (10) and (12), the following can be obtained:

$$\begin{aligned} &\iint_\Omega udiv\vec{\varphi}dxdy + \iint_\Omega \nabla u \bullet \vec{\varphi}dxdy \\ &= \iint_\Omega \left[\left(u\frac{\partial \varphi_x}{\partial x} + u\frac{\partial \varphi_y}{\partial y}\right) + \left(\frac{\partial u}{\partial x}\varphi_x + \frac{\partial u}{\partial y}\varphi_y\right)\right]dxdy \\ &= \iint_\Omega \left[\left(u\frac{\partial \varphi_x}{\partial x} + \frac{\partial u}{\partial x}\varphi_x\right) + \left(u\frac{\partial \varphi_y}{\partial y} + \frac{\partial u}{\partial y}\varphi_y\right)\right]dxdy \\ &= \iint_\Omega \left[\frac{\partial (u\varphi_x)}{\partial x} + \frac{\partial (u\varphi_y)}{\partial y}\right]dxdy, \end{aligned} \tag{13}$$

where Ω denotes a two-dimensional simply connected region. Further, the traditional first-order Green formula can be given as:

$$\oint_C P(x,y)dx + Q(x,y)dy = \iint_\Omega \left(\frac{\partial Q}{\partial x} - \frac{\partial P}{\partial y}\right)dxdy, \tag{14}$$

where C denotes the piecewise smooth boundary curve of Ω, $P(x, y)$ and $Q(x, y)$ are continuous both on C and Ω. Thus, from (13) and (14), it follows that:

$$\iint_\Omega udiv\vec{\varphi}dxdy + \iint_\Omega \nabla u \bullet \vec{\varphi}dxdy = \oint_C -u\varphi_y dx + u\varphi_x dy. \tag{15}$$

Without loss of generality, Ω bears a rectangular shape for most real applications, C is a rectangular boundary. Figure 1 shows the two-dimensional simply connected region of a rectangular region.

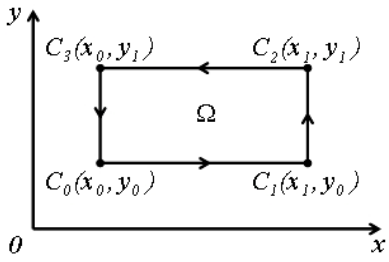

FIGURE 1. Two-dimensional simply connected region of a rectangular region.

Thus, from Figure 1 and (15), the following can be obtained:

$$\begin{aligned} &\iint_\Omega udiv\vec{\varphi}dxdy + \iint_\Omega \nabla u \bullet \vec{\varphi}dxdy \\ &= \oint_C -u\varphi_y dx + u\varphi_x dy \\ &= \int_{x_0}^{x_1} -u\varphi_y dx + \int_{y_0}^{y_1} u\varphi_x dy + \int_{x_1}^{x_0} -u\varphi_y dx + \int_{y_1}^{y_0} u\varphi_x dy \\ &= -\int_{x_0}^{x_1} u\varphi_y dx + \int_{y_0}^{y_1} u\varphi_x dy + \int_{x_0}^{x_1} u\varphi_y dx - \int_{y_0}^{y_1} u\varphi_x dy \\ &= 0. \end{aligned} \tag{16}$$

From (16), it follows that:

$$\begin{aligned} \iint_\Omega udiv\vec{\varphi}dxdy &= \iint_\Omega u(\nabla \bullet \vec{\varphi})dxdy \\ &= -\iint_\Omega \nabla u \bullet \vec{\varphi}dxdy \\ &= -\langle \nabla u, \vec{\varphi} \rangle \\ &= -\langle u, \nabla^* \vec{\varphi} \rangle \\ &= \iint_\Omega u(-\nabla^* \vec{\varphi})dxdy, \end{aligned} \tag{17}$$

where symbol $\langle , \rangle$ denotes the first-order inner product and ∇^* denotes the first-order Hilbert adjoint operator of a Hamilton operator ∇.

Note that from (17), the following is true:

$$div = -\nabla^*. \tag{18}$$

Equation (17) shows that to enable $-\iint_\Omega \nabla u \bullet \vec{\varphi}dxdy = 0$ be set up, a necessary condition can be given as:

$$\begin{aligned} \iint_\Omega udiv\vec{\varphi}dxdy &= \iint_\Omega \left(u\frac{\partial \varphi_x}{\partial x} + u\frac{\partial \varphi_y}{\partial y}\right)dxdy \\ &= 0. \end{aligned} \tag{19}$$

Because $u(x, y)$ is a test function, $u(x, y)$ is arbitrary. Therefore, according to the fundamental lemma of variation [6], [16], to enable (19) to be set up, a necessary condition can be given as:

$$\frac{\partial \varphi_x}{\partial x} + \frac{\partial \varphi_y}{\partial y} = 0. \tag{20}$$

Equation (20) shows that $\frac{\partial \varphi_x}{\partial x} + \frac{\partial \varphi_y}{\partial y} = 0$ is the first-order Euler-Lagrange equation of $-\iint_\Omega \nabla u \bullet \vec{\varphi}dxdy = 0$. This completes the proof.

Example 1: A first-order variational framework based on the first-order differential is given as:

$$\begin{cases} \text{Minimize}: \ E\left[u\left(x,y\right)\right] = \iint\limits_{\Omega} F\left(x,y,u,\dfrac{\partial u}{\partial x},\dfrac{\partial u}{\partial y}\right)dxdy \\ \text{Subject to}: \ \left\langle D^1 u, \vec{\boldsymbol{n}}\right\rangle = 0 \text{ on } \partial\Omega, \end{cases} \tag{21}$$

where E denotes an energy functional, $D^1 = \nabla$ denotes the first-order differential operator, $\vec{\boldsymbol{n}}$ denotes the normal to the boundary, $\partial\Omega$ denotes the boundary of Ω, and symbol $\langle,\rangle$ denotes the first-order Euclidean inner product. Equation (21) assumes that the function value of $u\left(x,y\right)$ continues smoothly as a constant beyond its boundaries. This artificial assumption is required for Neumann boundary condition that would have minor effect on the final results, i.e. the first-order directional derivative $\left\langle D^1 u, \vec{\boldsymbol{n}}\right\rangle = \langle \nabla u, \vec{\boldsymbol{n}}\rangle = \nabla u \bullet \vec{\boldsymbol{n}} = \dfrac{\partial u}{\partial \vec{\boldsymbol{n}}} = 0$. Suppose $u\left(x,y\right)$ is a first-order extremal surface of energy functional E, then $\xi(x,y) \in C_0^{\infty}\left(\Omega\right)$ is an admissible surface, a test function, closing to $u\left(x,y\right)$. $u\left(x,y\right)$ and $\xi(x,y)$ can be merged into a family of surfaces, $u+\beta\xi$, where β is a small parameter. When $\beta = 0$, the family of surfaces, $u+\beta\xi$, converts into the first-order extremal surface, $u\left(x,y\right)$. The first-order derivative of the extreme points equals to zero. Thus, the anisotropic diffusion of (21) can be explained as the first-order dissipation process of energy functional E. To achieve the first-order minimum of (21), a first-order energy functional on the family of surfaces, $u+\beta\xi$, is given as:

$$\begin{aligned} \delta E &= \frac{\partial}{\partial\beta}\iint\limits_{\Omega} \\ &\quad \times F\left[x,y,u\left(x,y,\beta\right),\frac{\partial u\left(x,y,\beta\right)}{\partial x},\frac{\partial u\left(x,y,\beta\right)}{\partial y}\right]dxdy \\ &= \iint\limits_{\Omega}\left(F_u\delta u + F_p\delta p + F_q\delta q\right)dxdy \\ &= \iint\limits_{\Omega}\left[F_u\delta u + \left(F_p,F_q\right)\bullet\left(\delta p,\delta q\right)\right]dxdy \\ &= \iint\limits_{\Omega}\left[F_u\delta u + \nabla\delta u\bullet\left(F_p,F_q\right)\right]dxdy \\ &= 0, \end{aligned} \tag{22}$$

where $F_u = \dfrac{\partial F}{\partial u}$, $\delta u = \dfrac{\partial u\left(x,y,\beta\right)}{\partial\beta}$, $p\left(x,y\right) = \dfrac{\partial u\left(x,y\right)}{\partial x}$, $q\left(x,y\right) = \dfrac{\partial u\left(x,y\right)}{\partial y}$, $\delta p = \dfrac{\partial p\left(x,y,\beta\right)}{\partial\beta}$, $\delta q = \dfrac{\partial q\left(x,y,\beta\right)}{\partial\beta}$, $u\left(x,y,\beta\right) = u\left(x,y\right) + \beta\delta u = u\left(x,y\right) + \beta\left[\xi\left(x,y\right) - u\left(x,y\right)\right]$, $p\left(x,y,\beta\right) = \dfrac{\partial u\left(x,y,\beta\right)}{\partial x} = p\left(x,y\right) + \beta\delta p$, and $q\left(x,y,\beta\right) = \dfrac{\partial u\left(x,y,\beta\right)}{\partial y} = q\left(x,y\right) + \beta\delta q$. Thus, from (8), (20), and (22), the following can be obtained:

$$\iint\limits_{\Omega}\left[F_u\delta u - div\left(F_p,F_q\right)\delta u\right]dxdy = 0. \tag{23}$$

Because δu is arbitrary, according to the fundamental lemma of variation [6], [16], to enable (23) to be set up, a necessary condition can be given as:

$$\begin{aligned} \left[F_u - div\left(F_p,F_q\right)\right] &= \left[F_u - \frac{\partial F_p}{\partial x} - \frac{\partial F_q}{\partial y}\right] \\ &= 0. \end{aligned} \tag{24}$$

Equation (24) shows that $\left[F_u - \dfrac{\partial F_p}{\partial x} - \dfrac{\partial F_q}{\partial y}\right] = 0$ is the first-order Euler-Lagrange equation of

$$\frac{\partial}{\partial\beta}\iint\limits_{\Omega} F\left[x,y,u(x,y,\beta),\frac{\partial u(x,y,\beta)}{\partial x},\frac{\partial u(x,y,\beta)}{\partial y}\right]dxdy\Bigg|_{\beta=0} = 0.$$

Thus, $u\left(x,y\right)$ is a solution of $\left[F_u - \dfrac{\partial F_p}{\partial x} - \dfrac{\partial F_q}{\partial y}\right] = 0$.

B. FRACTIONAL-ORDER EULER-LAGRANGE EQUATION BASED ON WIENER-KHINTCHINE THEOREM

In this subsection, based on Wiener-Khintchine theorem, the fractional-order Euler-Lagrange equation for the fractional-order variational method is derived. Bai and Feng [117], Guidotti and Lambers [118], and Zhang [119] claimed that the fractional-order Euler-Lagrange equation for the fractional-order variational method could be derived based on Parseval theorem. Note that Parseval theorem actually studies the relationship between a self-correlation function and a self-energy-density spectrum or a self-power-density spectrum of an identical continuously differentiable signal $s\left(t\right)$, which can be derived as $\frac{1}{2\pi}\int\limits_{-\infty}^{\infty} S\left(\mathrm{j}\omega\right)\overline{S\left(\mathrm{j}\omega\right)}d\omega = \int\limits_{-\infty}^{\infty} s^2\left(t\right)dt$, where $S\left(\mathrm{j}\omega\right)$ is the Fourier transforms of $s\left(t\right)$ and $\overline{S\left(\mathrm{j}\omega\right)}$ is the complex conjugation of $S\left(\mathrm{j}\omega\right)$. However, the derivation of the fractional-order Euler-Lagrange equation for the fractional-order variational method should simultaneously consider two different factors: a fractional-order extremal surface of energy functional and a closing admissible surface. The relationship between a cross-correlation function and a cross energy density spectrum or a cross power density spectrum of two different continuously differentiable signals need be discussed. Therefore, the fractional-order Euler-Lagrange equation for the fractional-order variational method should be derived based on Wiener-Khintchine theorem, rather than Parseval theorem.

Lemma 2: With regard to a v-order continuously differentiable scalar function $u(x,y)$ and a v-order continuously differentiable vector function $\vec{\boldsymbol{\varphi}} = \left(\varphi_x,\varphi_y\right)$, based on Wiener-Khintchine theorem, the fractional-order Euler-Lagrange equation of $\iint\limits_{\Omega} D^v u\bullet\vec{\boldsymbol{\varphi}}dxdy = 0$ can be derived as:

$$\frac{1}{4\pi^2}\mathrm{Re}\left(\overline{D_x^v}\varphi_x + \overline{D_y^v}\varphi_y\right) = 0, \tag{25}$$

where $u(x,y)$ is an admissible surface (a test function), Ω is an open bounded subsets of real plane R^2 with smooth bound-

ary, v is a real number, Re () computes the real part of the complex number, symbol $*$ denotes a linear convolution, and $\overline{D_x^v}$ and $\overline{D_y^v}$ denote the conjugate operators of the v-order partial differential operators D_x^v and D_y^v, respectively.

Proof: In view of signal processing, the cross-correlation function between continuous signal $s_1(t)$ and continuous signal $s_2(t)$ can be given as:

$$\begin{aligned} r_{12}(\tau) &= s_1(\tau) * \overline{s_2(-\tau)} \\ &= \int_{-\infty}^{\infty} s_1(t)\overline{s_2(t-\tau)}dt \\ &\underset{\text{are real signals.}}{\overset{\text{If } s_1(t) \text{ and } s_2(t)}{=}} s_1(\tau) * s_2(-\tau) \\ &= \int_{-\infty}^{\infty} s_1(t) s_2(t-\tau)\, dt, \end{aligned} \tag{26}$$

where $\overline{s_2(-\tau)}$ is the complex conjugation of $s_2(-\tau)$ and symbol $*$ denotes a linear convolution. Thus, whether $s_1(t)$ and $s_2(t)$ are real signals or not, the Fourier transform of (26) is as follows:

$$R_{12}(\mathrm{j}\omega) = S_1(\mathrm{j}\omega) * \overline{S_2(\mathrm{j}\omega)}, \tag{27}$$

where j denotes an imaginary unit, ω denotes an angular frequency, $\overline{S_2(\mathrm{j}\omega)}$ is the complex conjugation of $S_2(\mathrm{j}\omega)$, and $R_{12}(\mathrm{j}\omega)$, $S_1(\mathrm{j}\omega)$, and $S_2(\mathrm{j}\omega)$ are the Fourier transforms of $r_{12}(\tau)$, $s_1(t)$, and $s_2(t)$, respectively. Further, if $s_1(t)$ and $s_2(t)$ are real signals, from (26) and (27), Wiener-Khintchine theorem can be given as:

$$\begin{aligned} r_{12}(0) &= \frac{1}{2\pi}\int_{-\infty}^{\infty} S_1(\mathrm{j}\omega)\overline{S_2(\mathrm{j}\omega)}e^{\mathrm{j}\omega\tau}d\omega\Big|_{\tau=0} \\ &= \frac{1}{2\pi}\int_{-\infty}^{\infty} S_1(\mathrm{j}\omega)\overline{S_2(\mathrm{j}\omega)}d\omega \\ &= s_1(\tau) * s_2(-\tau)|_{\tau=0} \\ &= \int_{-\infty}^{\infty} s_1(t)\, s_2(t)\, dt. \end{aligned} \tag{28}$$

Equation (28) shows that first, $r_{12}(0)$ is equal to the cross energy or cross power between $s_1(t)$ and $s_2(t)$. Second, with regard to continuously differentiable signal, the relationship between a cross-correlation function and a cross energy density spectrum or a cross power density spectrum can be derived as $\frac{1}{2\pi}\int_{-\infty}^{\infty} S_1(\mathrm{j}\omega)\overline{S_2(\mathrm{j}\omega)}d\omega = \int_{-\infty}^{\infty} s_1(t)\, s_2(t)\, dt$. Therefore, from (28), $\iint_{\Omega} D^v u \bullet \vec{\varphi} dxdy$ can be rewritten (29), as shown at the bottom of this page, where $U(\mathrm{j}\omega_x, \mathrm{j}\omega_y)$, $\Phi_x(\mathrm{j}\omega_x, \mathrm{j}\omega_y)$, $\Phi_y(\mathrm{j}\omega_x, \mathrm{j}\omega_y)$, $(\mathrm{j}\omega_x)^v$, and $(\mathrm{j}\omega_y)^v$ are the Fourier transforms of $u(x, y)$, $\varphi_x(x, y)$, $\varphi_y(x, y)$, D_x^v, and D_y^v, respectively, Ω_ω is corresponding to Ω in the domain of Fourier transform, and $\overline{(\mathrm{j}\omega_x)^v}$, $\overline{(\mathrm{j}\omega_y)^v}$, and $\overline{U(\mathrm{j}\omega_x, \mathrm{j}\omega_y)}$ are the complex conjugations of $(\mathrm{j}\omega_x)^v$, $(\mathrm{j}\omega_y)^v$, and $U(\mathrm{j}\omega_x, \mathrm{j}\omega_y)$, respectively. Because $u(x, y)$ is a test function, $\overline{U(\mathrm{j}\omega_x, \mathrm{j}\omega_y)}$ is arbitrary. Therefore, according to the fundamental lemma of variation, to enable $\iint_{\Omega} D^v u \bullet \vec{\varphi} dxdy = 0$ to be set up, an essential condition can be given as:

$$\frac{1}{4\pi^2}\left[\overline{(\mathrm{j}\omega_x)^v}\Phi_x(\mathrm{j}\omega_x, \mathrm{j}\omega_y) + \overline{(\mathrm{j}\omega_y)^v}\Phi_y(\mathrm{j}\omega_x, \mathrm{j}\omega_y)\right] = 0. \tag{30}$$

The inverse Fourier transform of (30) is as follows:

$$\begin{aligned} &\frac{1}{4\pi^2}\mathrm{Re}\left[h_x^v(x, y) * \varphi_x + h_y^v(x, y) * \varphi_y\right] \\ &\quad = \frac{1}{4\pi^2}\mathrm{Re}\left(\overline{D_x^v}\varphi_x + \overline{D_y^v}\varphi_y\right) = 0, \end{aligned} \tag{31}$$

where Re () computes the real part of the complex number, $h_x^v(x, y) \overset{FT}{\leftrightarrow} \overline{(\mathrm{j}\omega_x)^v}$, $h_y^v(x, y) \overset{FT}{\leftrightarrow} \overline{(\mathrm{j}\omega_y)^v}$, and $\overline{D_x^v}$ and $\overline{D_y^v}$ denote the conjugate operators of the v-order partial differential operators D_x^v and D_y^v, respectively. The second item on the right side of (31), $\frac{1}{4\pi^2}\mathrm{Re}\left(\overline{D_x^v}\varphi_x + \overline{D_y^v}\varphi_y\right)$, is expressed in the form of operator. This completes the proof.

Note that first, the aforementioned proof can also be achieved by means of the theory of Hilbert adjoint operator [116]. The Hilbert adjoint operator of a fractional differential operator is a complex conjugate transpose matrix of that of the corresponding fractional differential operator. Second, because the inverse Fourier transforms of $(\mathrm{j}\omega_x)^v$ and $(\mathrm{j}\omega_y)^v$

$$\begin{aligned} \iint_{\Omega} D^v u \bullet \vec{\varphi} dxdy &= \iint_{\Omega} \vec{\varphi} \bullet D^v u dxdy \\ &= \iint_{\Omega} \left\{\varphi_x(x, y)\left[D_x^v u(x, y)\right] + \varphi_y(x, y)\left[D_y^v u(x, y)\right]\right\} dxdy \\ &= \frac{1}{4\pi^2}\iint_{\Omega_\omega} \left[\Phi_x(\mathrm{j}\omega_x, \mathrm{j}\omega_y)\overline{(\mathrm{j}\omega_x)^v U(\mathrm{j}\omega_x, \mathrm{j}\omega_y)} + \Phi_y(\mathrm{j}\omega_x, \mathrm{j}\omega_y)\overline{(\mathrm{j}\omega_y)^v U(\mathrm{j}\omega_x, \mathrm{j}\omega_y)}\right] d\omega_x d\omega_y \\ &= \frac{1}{4\pi^2}\iint_{\Omega_\omega} \left[\overline{(\mathrm{j}\omega_x)^v}\Phi_x(\mathrm{j}\omega_x, \mathrm{j}\omega_y)\overline{U(\mathrm{j}\omega_x, \mathrm{j}\omega_y)} + \overline{(\mathrm{j}\omega_y)^v}\Phi_y(\mathrm{j}\omega_x, \mathrm{j}\omega_y)\overline{U(\mathrm{j}\omega_x, \mathrm{j}\omega_y)}\right] d\omega_x d\omega_y, \end{aligned} \tag{29}$$

belong to Euler integral of the second kind, $\overline{D_x^v}$ and $\overline{D_y^v}$ could not be achieved in spatial domain or time domain directly, which should be implemented in discrete Fourier if transform domain. With regard to two-dimensional discrete signal $s(mT, nT)$, according to the period extend theory, its discrete Fourier transform and inverse discrete Fourier transform can be given as, respectively:

$$\begin{aligned} S(\alpha, \beta) &= S\left(\frac{2\pi}{MT}\alpha, \frac{2\pi}{NT}\beta\right) \\ &= \sum_{m=0}^{M-1}\sum_{n=0}^{N-1} s(mT, nT)\, e^{-\mathrm{j}2\pi\left(\frac{m\alpha}{M}+\frac{n\beta}{N}\right)}, \end{aligned} \tag{32}$$

$$s(mT, nT) = \frac{1}{MN}\sum_{u=0}^{M-1}\sum_{v=0}^{N-1} S(\alpha, \beta)\, e^{\mathrm{j}2\pi\left(\frac{m\alpha}{M}+\frac{n\beta}{N}\right)}, \tag{33}$$

where $m = 0, 1, \cdots, M-1$, $n = 0, 1, \cdots, N-1$, T is the interval between the discrete points, $S(\alpha, \beta)$ is the discrete Fourier transform of $s(mT, nT)$, $\alpha = 0, 1, \cdots, M-1$ and $\beta = 0, 1, \cdots, N-1$ in (32), and $m = 0, 1, \cdots, M-1$ and $n = 0, 1, \cdots, N-1$ in (33). Note that in signal processing and image processing, one usually use the notation of $s(,)$, the lowercase of "s", as a signal in time or space domain, while use the notation of $S(,)$, the uppercase of "s", as the corresponding signal in frequency domain. With regard to digital image processing, we have $T = 1$. From (32) and (33), the first-order difference operators, d_x^1 and d_y^1, of $s(mT, nT)$ can be derived as, respectively:

$$\begin{aligned} &d_x^1 s(mT, nT) \\ &\quad = s(mT, nT) - s[(m-1)T, nT] \\ &\quad = \frac{1}{MN}\sum_{u=0}^{M-1}\sum_{v=0}^{N-1} S(\alpha, \beta)\left(1 - e^{\mathrm{j}\frac{2\pi\alpha}{M}}\right) e^{\mathrm{j}\left(\frac{m\alpha}{M}+\frac{n\beta}{N}\right)}, \end{aligned} \tag{34}$$

$$\begin{aligned} &d_y^1 s(mT, nT) \\ &\quad = s(mT, nT) - s[mT, (n-1)T] \\ &\quad = \frac{1}{MN}\sum_{u=0}^{M-1}\sum_{v=0}^{N-1} S(\alpha, \beta)\left(1 - e^{\mathrm{j}\frac{2\pi\beta}{N}}\right) e^{\mathrm{j}\left(\frac{m\alpha}{M}+\frac{n\beta}{N}\right)}. \end{aligned} \tag{35}$$

Thus, by means of mathematical induction, from (34) and (35), the *nth*-order difference operators, d_x^n and d_y^n, of can be derived as, respectively:

$$d_x^n \overset{DFT}{\leftrightarrow} \left(1 - e^{\mathrm{j}\frac{2\pi\alpha}{M}}\right)^n, \tag{36}$$

$$d_y^n \overset{DFT}{\leftrightarrow} \left(1 - e^{\mathrm{j}\frac{2\pi\beta}{N}}\right)^n, \tag{37}$$

where DFT denotes discrete Fourier transform. Then, extending (36) and (37) from the integer-order to fractional-order, the v-order difference operators, d_x^v and d_y^v, can be derived as:

$$D_x^v \approx d_x^v \overset{DFT}{\leftrightarrow} \left(1 - e^{\mathrm{j}\frac{2\pi\alpha}{M}}\right)^v, \tag{38}$$

$$D_y^v \approx d_y^v \overset{DFT}{\leftrightarrow} \left(1 - e^{\mathrm{j}\frac{2\pi\beta}{N}}\right)^v. \tag{39}$$

Thus, from (38) and (39), the following can be obtained:

$$\overline{D_x^v} \approx \overline{d_x^v} \overset{DFT}{\leftrightarrow} \overline{\left(1 - e^{\mathrm{j}\frac{2\pi\alpha}{M}}\right)^v}, \tag{40}$$

$$\overline{D_y^v} \approx \overline{d_y^v} \overset{DFT}{\leftrightarrow} \overline{\left(1 - e^{\mathrm{j}\frac{2\pi\beta}{N}}\right)^v}, \tag{41}$$

where $\alpha = 0, 1, \cdots, M-1$, $\beta = 0, 1, \cdots, N-1$, and $\overline{d_x^v}$ and $\overline{d_y^v}$ are the conjugate operators of d_x^v and d_y^v, respectively. Third, from aforementioned discussion, we can see that the fractional-order Euler-Lagrange equation based on Wiener-Khintchine theorem should be achieved by discrete Fourier transform and inverse discrete Fourier transform successively, which is difficult and complex to implement.

C. FRACTIONAL-ORDER EULER-LAGRANGE EQUATION BASED ON FRACTIONAL-ORDER GREEN FORMULA

In this subsection, in order to directly and easily implement the fractional-order variational method in spatial domain or time domain, the fractional-order Green formula and the fractional-order Euler-Lagrange equation based on the fractional-order Green formula are proposed, respectively.

At first, in order to derive the fractional-order Euler-Lagrange equation, the traditional first-order Green formula should be extended firstly from the first-order one to the fractional-order one.

A two-dimensional simply connected region can be shown as given in Figure 2.

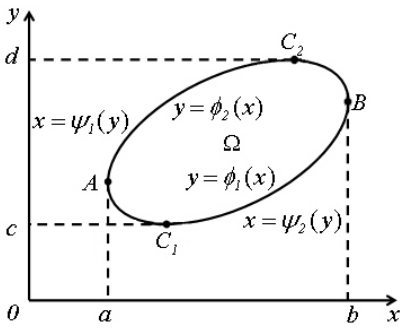

FIGURE 2. A two-dimensional simply connected region.

As shown in Figure 2, Ω is a two-dimensional simply connected region, C is the piecewise smooth boundary curve of Ω, and C consists of two piecewise smooth boundary curves, i.e. $y = \varphi_1(x), y = \varphi_2(x), a \le x \le b$ and $x = \psi_1(y), x = \psi_2(y), c \le y \le d$. For the convenience of illustration, let us sign the first-order differential operator, the v-order fractional differential operator, the first-order integral operator, the v-order fractional integral operator, the v-order fractional surface integral operator on Ω, the v-order fractional line integral operator on the AC_1B segment of C along the direction of $\overrightarrow{AC_1B}$, and the v-order fractional line integral operator on closed curve C in counter-clockwise direction as the symbols of D^1, D^v, I^1, $I^v = D^{-v}$, $I_x^v I_y^v$, $\underset{\Omega}{I^v}$, $\underset{C(AC_1B)}{I^v}$, and $I_{C_1}^v$, respectively. Further, let $v > 0$ in the following derivation.

With regard to a differintegrable function [30] $P(x, y)$, if $P - D^{-v_1}D^{v_1}P \neq 0$, the following can be obtained:

$$D^{v_1}D^{v_2}P = D^{v_1+v_2}P - D^{v_1+v_2}\left(P - D^{-v_1}D^{v_1}P\right). \tag{42}$$

$$
\begin{aligned}
\underset{\Omega}{I_x^{v_2} I_y^{v_2}}\, D_y^{v_1} P(x,y) &= {}_a^b I_x^{v_2} {}_{\varphi_1(x)}^{\varphi_2(x)} I_y^{v_2} D_y^{v_1} P(x,y) \\
&= {}_a^b I_x^{v_2} \left\{ D_y^{v_1-v_2} P(x,y) - D_y^{v_1-v_2} \left[P(x,y) - D_y^{-v_1} D_y^{v_1} P(x,y) \right] \right\} \Big|_{\varphi_1(x)}^{\varphi_2(x)} \\
&= -\underset{C(BC_2A)}{I_x^{v_2}} \left\{ D_y^{v_1-v_2} P(x,y) - D_y^{v_1-v_2} \left[P(x,y) - D_y^{-v_1} D_y^{v_1} P(x,y) \right] \right\} \\
&\quad - \underset{C(AC_1B)}{I_x^{v_2}} \left\{ D_y^{v_1-v_2} P(x,y) - D_y^{v_1-v_2} \left[P(x,y) - D_y^{-v_1} D_y^{v_1} P(x,y) \right] \right\} \\
&= -\underset{C-}{I_x^{v_2}} \left\{ D_y^{v_1-v_2} P(x,y) - D_y^{v_1-v_2} \left[P(x,y) - D_y^{-v_1} D_y^{v_1} P(x,y) \right] \right\}. \qquad (44)
\end{aligned}
$$

$$
\begin{aligned}
\underset{\Omega}{I_x^{v_2} I_y^{v_2}} \left[D_x^{v_1} Q(x,y) - D_y^{v_1} P(x,y) \right] &= \underset{C-}{I_x^{v_2}} \left\{ D_y^{v_1-v_2} P(x,y) - D_y^{v_1-v_2} \left[P(x,y) - D_y^{-v_1} D_y^{v_1} P(x,y) \right] \right\} \\
&\quad + \underset{C-}{I_y^{v_2}} \left\{ D_x^{v_1-v_2} Q(x,y) - D_x^{v_1-v_2} \left[Q(x,y) - D_x^{-v_1} D_x^{v_1} Q(x,y) \right] \right\}. \qquad (46)
\end{aligned}
$$

Then, from (42), the following is true:

$$
\begin{aligned}
&I_x^{v_2} I_y^{v_2} D_y^{v_1} P(x,y) \\
&= I_x^{v_2} \left\{ D_y^{v_1-v_2} P(x,y) - D_y^{v_1-v_2} \left[P(x,y) - D_y^{-v_1} D_y^{v_1} P(x,y) \right] \right\}. \qquad (43)
\end{aligned}
$$

Therefore, from Figure 2 and (43), it follows that (44), as shown at the top of this page.

Likewise, with regard to a differintegrable function [30] $Q(x,y)$, if $Q - D^{-v_1} D^{v_1} Q \neq 0$, the following can be obtained:

$$
\begin{aligned}
&\underset{\Omega}{I_x^{v_2} I_y^{v_2}}\, D_x^{v_1} Q(x,y) \\
&= \underset{C-}{I_y^{v_2}} \left\{ D_x^{v_1-v_2} Q(x,y) - D_x^{v_1-v_2} \left[Q(x,y) - D_x^{-v_1} D_x^{v_1} Q(x,y) \right] \right\}. \qquad (45)
\end{aligned}
$$

Thus, from (44) and (45), the fractional-order Green formula can be derived (46), as shown at the bottom of this page.

If D^{-v_1} is the inverse operator of D^{v_1}, (42) can be simplified as $D^{v_1} D^{v_2} = D^{v_1+v_2}$. Then, (46) can be simplified as:

$$
\begin{aligned}
&\underset{\Omega}{I_x^{v_2} I_y^{v_2}} \left[D_x^{v_1} Q(x,y) - D_y^{v_1} P(x,y) \right] \\
&\quad = \underset{C-}{I_x^{v_2}}\, D_y^{v_1-v_2} P(x,y) + \underset{C-}{I_y^{v_2}}\, D_x^{v_1-v_2} Q(x,y). \qquad (47)
\end{aligned}
$$

Equation (47) shows that first, if $v_1 = v_2 = v$, (47) can be further simplified as:

$$
\underset{\Omega}{I_x^{v} I_y^{v}} \left[D_x^{v} Q(x,y) - D_y^{v} P(x,y) \right] = \underset{C-}{I_x^{v}}\, P(x,y) + \underset{C-}{I_y^{v}}\, Q(x,y). \qquad (48)
$$

Equation (48) has the same derived result as that of the literature [120]. Second, if $v_1 = v_2 = 1$, (47) can be further simplified as:

$$
\underset{\Omega}{I_x^{1} I_y^{1}} \left[D_x^{1} Q(x,y) - D_y^{1} P(x,y) \right] = \underset{C-}{I_x^{1}}\, P(x,y) + \underset{C-}{I_y^{1}}\, Q(x,y). \qquad (49)
$$

Compared with (14) and (49), we can see that two formulae are identical. In other words, the traditional first-order Green formula is actually a special case of the fractional-order Green formula.

In addition, let us sign the boundary curve surface of a three-dimensional region Ω as the symbols of S, and suppose the boundary curve C of S is piecewise smooth. In a similar way, if differintegrable function [30] $P(x,y,z)$, $Q(x,y,z)$, and $R(x,y,z)$ are the fractional-order continuously differentiable with respect to x, y, and z in Ω, on S, or on C, the fractional-order Gauss formula and the fractional-order Stokes formula can be derived as (50) and (51), as shown at the top of the next page.

It can be easily proved that the traditional first-order Gauss formula and the traditional first-order Stokes formula are actually a special case of the fractional-order Gauss formula and that of the fractional-order Stokes formula, respectively.

Secondly, based on the proposed fractional-order Green formula, the fractional-order Euler-Lagrange equation for the fractional-order variational method is proposed.

Lemma 3: With regard to a fractional-order continuously differentiable scalar function $u(x,y)$ and a fractional-order continuous differentiable vector function $\vec{\varphi} = (\varphi_x, \varphi_y)$, based on the fractional-order Green formula, an identical equation for the fractional-order variational method can be derived as:

$$
\begin{aligned}
-\underset{\Omega}{I_x^{v_2} I_y^{v_2}}\, D^{v_1} u \bullet \vec{\varphi} &= -\underset{\Omega}{I_x^{v_2} I_y^{v_2}} \left[\left(D_x^{v_1} u \right) \varphi_x + \left(D_y^{v_1} u \right) \varphi_y \right] \\
&= \underset{\Omega}{I_x^{v_2} I_y^{v_2}} \sum_{n=1}^{\infty} \binom{v_1}{n} \left[\left(D_x^{v_1-n} u \right) D_x^n \varphi_x + \left(D_y^{v_1-n} u \right) D_y^n \varphi_y \right]. \qquad (52)
\end{aligned}
$$

where $u(x,y)$ is an admissible surface (a test function), Ω is an open bounded subsets of real plane R^2 with smooth boundary, Ω bears a rectangular shape for most real applications, v_1 and v_2 are two real numbers, symbol $\bullet$ denotes the first-order Euclidean inner product. Note that $\frac{\Gamma(1+v_1)}{\Gamma(v_1)} [D_x^1 \varphi_x + D_y^1 \varphi_y] = 0$ is the fractional-order Euler-Lagrange equation of $-\underset{\Omega}{I_x^{v_2} I_y^{v_2}}\, D^{v_1} u \bullet \vec{\varphi} = 0$.

$$
\begin{aligned}
&\underset{\Omega}{I_x^{v_2} I_y^{v_2} I_z^{v_2}} \left(D_x^{v_1} P + D_y^{v_1} Q + D_z^{v_1} R\right) \\
&\quad = \underset{S}{I_y^{v_2} I_z^{v_2}} \left\{D_x^{v_1 - v_2} P - D_x^{v_1 - v_2}\left[P - D_x^{-v_1} D_x^{v_1} P\right]\right\} + \underset{S}{I_x^{v_2} I_z^{v_2}} \left\{D_y^{v_1 - v_2} Q - D_y^{v_1 - v_2}\left[Q - D_y^{-v_1} D_y^{v_1} Q\right]\right\} \\
&\qquad + \underset{S}{I_x^{v_2} I_y^{v_2}} \left\{D_z^{v_1 - v_2} R - D_z^{v_1 - v_2}\left[R - D_z^{-v_1} D_z^{v_1} R\right]\right\}, \qquad (50)
\end{aligned}
$$

$$
\begin{aligned}
&\underset{\Omega}{I_y^{v_2} I_z^{v_2}} \left(D_y^{v_1} R - D_z^{v_1} Q\right) + \underset{\Omega}{I_x^{v_2} I_z^{v_2}} \left(D_z^{v_1} P - D_x^{v_1} R\right) + \underset{\Omega}{I_x^{v_2} I_y^{v_2}} \left(D_x^{v_1} Q - D_y^{v_1} P\right) \\
&\quad = \frac{1}{2} \underset{C}{I_x^{v_2}} \left\{D_y^{v_1 - v_2} P - D_y^{v_1 - v_2}[P - D_y^{-v_1} D_y^{v_1} P] + D_z^{v_1 - v_2} P - D_z^{v_1 - v_2}[P - D_z^{-v_1} D_z^{v_1} P]\right\} \\
&\qquad + \frac{1}{2} \underset{C}{I_y^{v_2}} \left\{D_x^{v_1 - v_2} Q - D_x^{v_1 - v_2}[Q - D_x^{-v_1} D_x^{v_1} Q] + D_z^{v_1 - v_2} Q - D_z^{v_1 - v_2}[Q - D_z^{-v_1} D_z^{v_1} Q]\right\} \\
&\qquad + \frac{1}{2} \underset{C}{I_z^{v_2}} \left\{D_x^{v_1 - v_2} R - D_x^{v_1 - v_2}[R - D_x^{-v_1} D_x^{v_1} R] + D_y^{v_1 - v_2} R - D_y^{v_1 - v_2}[R - D_y^{-v_1} D_y^{v_1} R]\right\}. \qquad (51)
\end{aligned}
$$

Proof: Let us sign the v-order fractional differential operator as a symbol of $D^v = (D_x^v, D_y^v)$. If $v = 0$, D^0 represents an identity operator. Ω bears a rectangular shape for most real applications, C is a rectangular boundary, which can be shown as given in Figure 1. With regard to a causal signal, from (2), the following can be obtained, respectively:

$$
I_x^v s(x, y) = \frac{1}{\Gamma(v)} \int_{a_x}^{x} (x - \eta)^{v-1} s(\eta, y) d\eta, \qquad (53)
$$

$$
I_y^v s(x, y) = \frac{1}{\Gamma(v)} \int_{a_y}^{y} (y - \zeta)^{v-1} s(x, \zeta) d\zeta, \qquad (54)
$$

$$
I_x^v I_y^v s(x, y) = \frac{1}{\Gamma^2(v)} \int_{a_x}^{x} \int_{a_y}^{y} (x - \eta)^{v-1} (y - \zeta)^{v-1} s(\eta, \zeta) d\eta d\zeta. \qquad (55)
$$

Thus, with regard to a rectangular region Ω, from (46), (53)-(55), and Figure 1, it follows as (56), as shown at the bottom of this page.

Further, $\sum_{m=0}^{\infty} \sum_{n=0}^{m} \equiv \sum_{n=0}^{\infty} \sum_{m=n}^{\infty}$ and $\binom{v}{r+n}\binom{r+n}{n} \equiv \binom{v}{n}\binom{v-n}{r}$ can be derived, where v is a real number. Thus, from (1), it follows that [121]:

$$
D_{x-a}^v (fg) = \sum_{n=0}^{\infty} \left[\binom{v}{n} \left(D_{x-a}^{v-n} f\right) D_{x-a}^n g\right], \qquad (57)
$$

where $\binom{v}{n} = \frac{(-1)^n \Gamma(n - v)}{\Gamma(-v)\Gamma(1 + n)} = \frac{\Gamma(1 + v)}{\Gamma(1 - n + v)\Gamma(1 + n)}$. Moreover, according to the homogeneous properties of fractional calculus [30], from (56) and (57), the following can be obtained:

$$
\begin{aligned}
&\underset{\Omega}{I_x^{v_2} I_y^{v_2}} \left[D_x^{v_1}(u\varphi_x) + D_y^{v_1}(u\varphi_y)\right] \\
&\quad = \underset{\Omega}{I_x^{v_2} I_y^{v_2}} \left[D_x^{v_1}(u\varphi_x) - D_y^{v_1}(-u\varphi_y)\right] \\
&\quad = \underset{\Omega}{I_x^{v_2} I_y^{v_2}} \sum_{n=0}^{\infty} \binom{v_1}{n} \left[\left(D_x^{v_1 - n} u\right) D_x^n \varphi_x + \left(D_y^{v_1 - n} u\right) D_y^n \varphi_y\right] \\
&\quad = 0. \qquad (58)
\end{aligned}
$$

Thus, from (58), the following is true:

$$
\begin{aligned}
-\underset{\Omega}{I_x^{v_2} I_y^{v_2}} D^{v_1} u \bullet \vec{\varphi} &= -\underset{\Omega}{I_x^{v_2} I_y^{v_2}} \left[\left(D_x^{v_1} u\right)\varphi_x + \left(D_y^{v_1} u\right)\varphi_y\right] \\
&= \underset{\Omega}{I_x^{v_2} I_y^{v_2}} \sum_{n=1}^{\infty} \binom{v_1}{n} \left[\left(D_x^{v_1 - n} u\right) D_x^n \varphi_x + \left(D_y^{v_1 - n} u\right) D_y^n \varphi_y\right], \qquad (59)
\end{aligned}
$$

$$
\begin{aligned}
&\underset{\Omega}{I_x^{v_2} I_y^{v_2}} \left(D_x^{v_1} Q(x, y) - D_y^{v_1} P(x, y)\right) \\
&\quad = \underset{C-}{I_x^{v_2}} \left\{D_y^{v_1 - v_2} P(x, y) - D_y^{v_1 - v_2}[P(x, y) - D_y^{-v_1} D_y^{v_1} P(x, y)]\right\} + \underset{C-}{I_y^{v_2}} \left\{D_x^{v_1 - v_2} Q(x, y) - D_x^{v_1 - v_2}[Q(x, y) - D_x^{-v_1} D_x^{v_1} Q(x, y)]\right\} \\
&\quad = {}_{x_0}^{x_1} I_x^{v_2} \left\{D_y^{v_1 - v_2} P - D_y^{v_1 - v_2}[P - D_y^{-v_1} D_y^{v_1} P]\right\} + {}_{x_1}^{x_0} I_x^{v_2} \left\{D_y^{v_1 - v_2} P - D_y^{v_1 - v_2}[P - D_y^{-v_1} D_y^{v_1} P]\right\} \\
&\qquad + {}_{y_0}^{y_1} I_y^{v_2} \left\{D_x^{v_1 - v_2} Q - D_x^{v_1 - v_2}[Q - D_x^{-v_1} D_x^{v_1} Q]\right\} + {}_{y_1}^{y_0} I_y^{v_2} \left\{D_x^{v_1 - v_2} Q - D_x^{v_1 - v_2}[Q - D_x^{-v_1} D_x^{v_1} Q]\right\} \\
&\quad = 0. \qquad (56)
\end{aligned}
$$

where $\binom{v}{0} = \frac{\Gamma(1+v)}{\Gamma(1+v)\Gamma(1)} = 1$. From (59), if $-I_x^{v_2} I_y^{v_2} D^{v_1} u \bullet \vec{\varphi} = 0$, one can obtain:

$$\begin{aligned} &-I_x^{v_2} I_y^{v_2} D^{v_1} u \bullet \vec{\varphi} \\ &= I_x^{v_2} I_y^{v_2} \sum_{n=1}^{\infty} \binom{v_1}{n} \left[\left(D_x^{v_1-n} u \right) D_x^n \varphi_x + \left(D_y^{v_1-n} u \right) D_y^n \varphi_y \right] \\ &= 0. \end{aligned} \tag{60}$$

Since a vector in x direction and a vector in y direction are orthogonal to each other, to enable (60) be set up, a necessary condition can be given as:

$$\begin{cases} I_x^{v_2} I_y^{v_2} \sum_{n=1}^{\infty} \binom{v_1}{n} \left[\left(D_x^{v_1-n} u \right) D_x^n \varphi_x \right] = 0 \\ I_x^{v_2} I_y^{v_2} \sum_{n=1}^{\infty} \binom{v_1}{n} \left[\left(D_y^{v_1-n} u \right) D_y^n \varphi_y \right] = 0. \end{cases} \tag{61}$$

Because $u(x, y)$ is a test function, $D_x^{v_1-n} u(x, y)$ and $D_y^{v_1-n} u(x, y)$ are arbitrary. Therefore, to enable (60) to be set up, from (61), an essential condition can be given as:

$$\begin{cases} \binom{v_1}{n} D_x^n \varphi_x \overset{n=1\to\infty}{=} 0 \\ \binom{v_1}{n} D_y^n \varphi_y \overset{n=1\to\infty}{=} 0. \end{cases} \tag{62}$$

For n is a positive integer within $1 \to \infty$, to enable $\left(D_x^n \varphi_x, D_y^n \varphi_y \right) \overset{n=1\to\infty}{=} (0, 0)$ to be set up, only if $\left(D_x^1 \varphi_x, D_y^1 \varphi_y \right) = (0, 0)$ is satisfied. Thus, to enable (62) to be set up, only if $\begin{cases} \binom{v_1}{1} D_x^1 \varphi_x = 0 \\ \binom{v_1}{1} D_y^1 \varphi_y = 0 \end{cases}$ is satisfied. Further, to enable $\begin{cases} \binom{v_1}{1} D_x^1 \varphi_x = 0 \\ \binom{v_1}{1} D_y^1 \varphi_y = 0 \end{cases}$ to be set up, an essential condition can be given as $\binom{v_1}{1} \left(D_x^1 \varphi_x + D_y^1 \varphi_y \right) = 0$. Therefore, to enable (60) be set up, an essential condition can be given as:

$$\begin{aligned} \binom{v_1}{1} [D_x^1 \varphi_x + D_y^1 \varphi_y] &= \frac{\Gamma(1+v_1)}{\Gamma(v_1)} [D_x^1 \varphi_x + D_y^1 \varphi_y] \\ &= 0. \end{aligned} \tag{63}$$

Equation (63) shows that $\frac{\Gamma(1+v_1)}{\Gamma(v_1)} [D_x^1 \varphi_x + D_y^1 \varphi_y] = 0$ is the fractional-order Euler-Lagrange equation of $-I_x^{v_2} I_y^{v_2} D^{v_1} u \bullet \vec{\varphi} = 0$. Equation (63) is an equivalent equation of (31), which can be directly and easily implemented in spatial domain or time domain.

Note that first, $\frac{\Gamma(1+v_1)}{\Gamma(v_1)} [D_x^1 \varphi_x + D_y^1 \varphi_y] = 0$ is the fractional-order Euler-Lagrange equation of $-I_x^{v_2} I_y^{v_2} D^{v_1} u \bullet \vec{\varphi} = 0$, which is irrelevant to the order v_2 of fractional integral $I_x^{v_2} I_y^{v_2}$. Thus, let $v_2 = 1$ for most real applications. Second, if $v_1 = v_2 = 1$, $\frac{\Gamma(1+v_1)}{\Gamma(v_1)} \overset{v_1=1}{=} \frac{\Gamma(2)}{\Gamma(1)} = 1$. Thus, (63) can be simplified as:

$$D_x^1 \varphi_x + D_y^1 \varphi_y = 0. \tag{64}$$

Equation (64) is the first-order Euler-Lagrange equation of $-I_x^1 I_y^1 D^1 u \bullet \vec{\varphi} = 0$. Compared with (20) and (64), we can see that two formulae are identical. In other words, the traditional first-order Euler-Lagrange equation is actually a special case of the fractional-order Euler-Lagrange equation. This completes the proof.

Example 2: Because the traditional first-order Euler-Lagrange equation is actually a special case of the fractional-order Euler-Lagrange equation, the proposed fractional-order Euler-Lagrange equation can also be used to solve the classical issue of for the first-order variational method. The purpose of Example 2 is to verify directly that when we utilize the proposed fractional-order Euler-Lagrange equation based on fractional-order Green formula to deal with the classical first-order image restoration, it has the same results as those obtained by the classical first-order Euler-Lagrange equation, which is a concerned issue in image processing.

Let us suppose that $\Phi_1 (D^{v_1} u)$ is the corresponding scalar function of a scalar function u and $\Phi_2 (\vec{\varphi})$ is the corresponding scalar function of a vector function $\vec{\varphi}(x, y) = (\varphi_x, \varphi_y)$. Thus, if $-I_x^{v_2} I_y^{v_2} \left[\Phi_1 (D^{v_1} u) \Phi_2 (\vec{\varphi}) D^{v_1} u \right] \bullet \vec{\varphi} = 0$, from (59), (60), and (63), it follows as (65), as shown at the bottom of this page.

To enable (65) be set up, from (63), an essential condition can be given as:

$$\begin{aligned} &\binom{v_1}{1} \left\{ D_x^1 \left[\Phi_2 (\vec{\varphi}) \varphi_x \right] + D_y^1 \left[\Phi_2 (\vec{\varphi}) \varphi_y \right] \right\} \\ &= \frac{\Gamma(1+v_1)}{\Gamma(v_1)} \left\{ D_x^1 \left[\Phi_2 (\vec{\varphi}) \varphi_x \right] + D_y^1 \left[\Phi_2 (\vec{\varphi}) \varphi_y \right] \right\} = 0. \end{aligned} \tag{66}$$

$$\begin{aligned} &-I_x^{v_2} I_y^{v_2} \left[\Phi_1 \left(D^{v_1} u \right) \Phi_2 (\vec{\varphi}) D^{v_1} u \right] \bullet \vec{\varphi} \\ &= -I_x^{v_2} I_y^{v_2} \Phi_1 \left(D^{v_1} u \right) \left\{ D^{v_1} u \bullet \left[\Phi_2 (\vec{\varphi}) \vec{\varphi} \right] \right\} \\ &= I_x^{v_2} I_y^{v_2} \sum_{n=1}^{\infty} \binom{v_1}{n} \left\{ \left[\Phi_1 \left(D^{v_1} u \right) D_x^{v_1-n} u \right] D_x^n \left[\Phi_2 (\vec{\varphi}) \varphi_x \right] + \left[\Phi_1 \left(D^{v_1} u \right) D_y^{v_1-n} u \right] D_y^n \left[\Phi_2 (\vec{\varphi}) \varphi_y \right] \right\} \\ &= 0. \end{aligned} \tag{65}$$

Equation (66) shows that $\frac{\Gamma(1+v_1)}{\Gamma(v_1)}\{D_x^1[\Phi_2(\vec{\varphi})\varphi_x] + D_y^1[\Phi_2(\vec{\varphi})\,\varphi_y]\} = 0$ is the fractional-order Euler-Lagrange equation of $-I_x^{v_2}I_y^{v_2}\left[\Phi_1\left(D^{v_1}u\right)\Phi_2\left(\vec{\varphi}\right)D^{v_1}u\right]\bullet\vec{\varphi} = 0$.

Furthermore, in order to utilize the proposed fractional-order Euler-Lagrange equation based on fractional-order Green formula to deal with the classical first-order image restoration, we should construct a fractional-order energy functional in the first place. Without loss of generality, the fractional-order energy functional can be defined by:

$$\begin{aligned} E(u) &= \frac{1}{2}\underset{\Omega}{I_x^1 I_y^1}\left|D^{v_1}u\right|^{v_2} + \frac{\lambda}{2}\underset{\Omega}{I_x^1 I_y^1}(u-u_0)^2 \\ &= \frac{1}{2}\iint_\Omega \left|D^{v_1}u\right|^{v_2}dxdy + \frac{\lambda}{2}\iint_\Omega (u-u_0)^2\,dxdy, \end{aligned} \quad (67)$$

where u denotes a clean image, u_0 denotes a noisy image, λ denotes a regularization parameter, and Ω denotes the two-dimensional simply connected region of an image. Suppose that u is a first-order extremal surface of $E(u)$, $\xi(x,y) \in C_0^\infty(\Omega)$ is an admissible surface, a test function, closing to u. u and ξ can be merged into a family of surfaces, $u+\beta\xi$, where β is a small parameter. Then, when $\beta = 0$, the family of surfaces, $u+\beta\xi$, converts into the first-order extremal surface, u. This process of seeking the first-order extreme value of a fractional-order norm can be described as a first-order isotropic diffusion. Thus, from (67), the functional on a family of surfaces, $u+\beta\xi$ is given as:

$$\begin{aligned} F(\beta) &= \underset{\Omega}{I_x^1 I_y^1}\left[\frac{1}{2}\left|D^{v_1}u+\beta D^{v_1}\xi\right|^{v_2} + \frac{\lambda}{2}(u+\beta\xi-u_0)^2\right] \\ &= \frac{1}{2}\iint_\Omega \left|D^{v_1}u+\beta D^{v_1}\xi\right|^{v_2}dxdy \\ &\quad + \frac{\lambda}{2}\iint_\Omega (u+\beta\xi-u_0)^2\,dxdy, \end{aligned} \quad (68)$$

where $\iint_\Omega (u-u_0)^2 dxdy$ is the variance of image noise and $\frac{\lambda}{2}\iint_\Omega (u-u_0)^2 dxdy$ is a fidelity term. For the first item on the right side of (68), according to the linearity of the first-order calculus, one can obtain:

$$\begin{aligned} &D_\beta^1 \frac{1}{2}\underset{\Omega}{I_x^1 I_y^1}\left(\left|D^{v_1}u+\beta D^{v_1}\xi\right|^{v_2}\right)\Big|_{\beta=0} \\ &= \frac{1}{2}\underset{\Omega}{I_x^1 I_y^1}\,D_\beta^1\left(\left|D^{v_1}u+\beta D^{v_1}\xi\right|^{v_2}\right)\Big|_{\beta=0} \\ &= \frac{1}{2}\iint_\Omega \left(v_2\left|D^{v_1}u\right|^{v_2-2}D^{v_1}u\right)\bullet D^{v_1}\xi\,dxdy \\ &= 0. \end{aligned} \quad (69)$$

In addition, for the second item on the right side of (68), according to the linearity of the first-order calculus, we have:

$$\begin{aligned} &D_\beta^1\,\underset{\Omega}{I_x^1 I_y^1}\frac{\lambda}{2}(u+\beta\xi-u_0)^2\Big|_{\beta=0} \\ &= \underset{\Omega}{I_x^1 I_y^1}\,D_\beta^1\left[\frac{\lambda}{2}(u+\beta\xi-u_0)^2\right]\Big|_{\beta=0} \\ &= \iint_\Omega \lambda(u-u_0)\xi\,dxdy \\ &= 0. \end{aligned} \quad (70)$$

For test function ξ is arbitrary, according to the fundamental lemma of variation [6], [16], from (68), (69), and (70), the first-order Euler-Lagrange formula of (67) can be derived as:

$$\begin{aligned} &-\frac{\Gamma(1+v_1)}{2\Gamma(v_1)}v_2\left[D_x^1\left(\left|D^{v_1}u\right|^{v_2-2}D_x^{v_1}u\right)\right. \\ &\left. + D_y^1\left(\left|D^{v_1}u\right|^{v_2-2}D_y^{v_1}u\right)\right] + \lambda(u-u_0) = 0. \end{aligned} \quad (71)$$

Equation (71) shows that $-\frac{\Gamma(1+v_1)}{2\Gamma(v_1)}v_2\left[D_x^1\left(\left|D^{v_1}u\right|^{v_2-2}D_x^{v_1}u\right) + D_y^1\left(\left|D^{v_1}u\right|^{v_2-2}D_y^{v_1}u\right)\right] + \lambda(u-u_0) = 0$ is the first-order Euler-Lagrange formula of $E(u) = \frac{1}{2}\iint_\Omega \left|D^{v_1}u\right|^{v_2}dxdy + \frac{\lambda}{2}\iint_\Omega (u-u_0)^2\,dxdy$.

In particular, first, if $v_1 = 1$ and $v_2 = 2$ in (67), a classical isotropic diffusion denoising model [18] can be given as:

$$E(u) = \frac{1}{2}\iint_\Omega \left|D^1u\right|^2 dxdy + \frac{\lambda}{2}\iint_\Omega (u-u_0)^2\,dxdy. \quad (72)$$

When $v_1 = 1$ and $v_2 = 2$, $\frac{\Gamma(1+v_1)}{2\Gamma(v_1)}v_2 \overset{v_1=1,v_2=2}{=\!=} \frac{\Gamma(2)}{\Gamma(1)} = 1$. Thus, in this case, (71) can be simplified as:

$$\begin{aligned} &-\left[D_x^1\left(D_x^1u\right) + D_y^1\left(D_y^1u\right)\right] + \lambda(u-u_0) \\ &= -D^1\bullet\left(D^1u\right) + \lambda(u-u_0) \\ &= -\nabla\bullet(\nabla u) + \lambda(u-u_0) \\ &= 0. \end{aligned} \quad (73)$$

Equation (73) is identical with the first-order Euler-Lagrange equation for a classical isotropic diffusion denoising model in the literatures of [18]. Second, if $v_1 = 1$ and $v_2 = 1$ in (67), a classical anisotropy diffusion denoising model, total variation (TV) denoising model [19], [20] can be given as:

$$E(u) = \iint_\Omega \left|D^1u\right|dxdy + \frac{\lambda}{2}\iint_\Omega (u-u_0)^2\,dxdy. \quad (74)$$

When $v_1 = 1$ and $v_2 = 1$, $\frac{\Gamma(1+v_1)}{\Gamma(v_1)} v_2 \overset{v_1=1, v_2=2}{=} \frac{\Gamma(2)}{\Gamma(1)} = 1$. Thus, in this case, (71) can be simplified as:

$$\begin{aligned} &-\left[D_x^1\left(\left|D^1u\right|^{-1} D_x^1u\right) + D_y^1\left(\left|D^1u\right|^{-1} D_y^1u\right)\right] + \lambda(u-u_0) \\ &\quad = -D^1 \bullet \left(\frac{D^1u}{|D^1u|}\right) + \lambda(u-u_0) \\ &\quad = -\nabla \bullet \left(\frac{\nabla u}{|D^1u|}\right) + \lambda(u-u_0) \\ &\quad = 0. \end{aligned} \tag{75}$$

Equation (75) is identical with the first-order Euler-Lagrange equation for a classical anisotropy diffusion denoising model in the literatures of [19] and [20]. Third, if $v_1 = 1$ and $v_2 = p$ in (67), a classical generalized total variation denoising model [21] can be given as:

$$E(u) = \frac{1}{p}\iint\limits_{\Omega} \left|D^1u\right|^p dxdy + \frac{\lambda}{2}\iint\limits_{\Omega} (u-u_0)^2\, dxdy. \tag{76}$$

When $v_1 = 1$ and $v_2 = p$, $\frac{\Gamma(1+v_1)}{p\Gamma(v_1)} v_2 \overset{v_1=1, v_2=p}{=} \frac{\Gamma(2)}{\Gamma(1)} = 1$. Thus, in this case, (71) can be simplified as:

$$\begin{aligned} &-\left[D_x^1\left(\left|D^1u\right|^{p-2} D_x^1u\right) + D_y^1\left(\left|D^1u\right|^{p-2} D_y^1u\right)\right] + \lambda(u-u_0) \\ &\quad = -D^1 \bullet \left(\left|D^1u\right|^{p-2} D^1u\right) + \lambda(u-u_0) \\ &\quad = -\nabla \bullet \left(|\nabla u|^{p-2}\nabla u\right) + \lambda(u-u_0) \\ &\quad = 0. \end{aligned} \tag{77}$$

Equation (77) is identical with the first-order Euler-Lagrange equation for a classical generalized total variation denoising model in the literatures of [21]. From (73), (75), and (77), we can see that when we utilize the proposed fractional-order Euler-Lagrange equation based on fractional-order Green formula to deal with the classical first-order image restoration problems, it has the same results as those obtained by the classical first-order Euler-Lagrange equation.

D. SOLUTION PROCEDURE OF FRACTIONAL-ORDER EULER-LAGRANGE EQUATION

In this subsection, the solution procedure of the fractional-order Euler-Lagrange equation is derived. In order to let this paper self-contained for a reader being not familiar with fractional calculus and the fractional-order gradient descent method, this subsection includes a brief necessary recall on the fractional-order time marching method.

At first, the solution procedure of the first-order Euler-Lagrange equation uses a parabolic equation with time as an evolution parameter (the time marching method), or equivalently, the first-order gradient descent method [18]. Note that, with regard to a two-dimensional signal such as an image, it is treated as a function of time and space, $u(x, y, t)$, and the time marching method is used to search the first-order steady state of (20). This means that for $I_x^1 I_y^1 D^1u \bullet \vec{\varphi} = 0$, we solve:

$$\frac{\partial u(x,y,t)}{\partial t} = \frac{\partial \varphi_x[u(x,y,t)]}{\partial x} + \frac{\partial \varphi_y[u(x,y,t)]}{\partial y}, \tag{78}$$

where $\vec{\varphi}(x, y, t) = (\varphi_x, \varphi_y) = \{\varphi_x[u(x, y, t)], \varphi_y[u(x, y, t)]\}$.

Secondly, in a similar way, the solution procedure of the fractional-order Euler-Lagrange equation also uses a parabolic equation with time as an evolution parameter (the time marching method), or equivalently, the fractional-order gradient descent method [73]. Note that, with regard to a two-dimensional signal such as an image, it is treated as a function of time and space, $u(x, y, t)$, and the time marching method is used to search the fractional-order steady state of (25) and (63), respectively. This means that for $\iint\limits_{\Omega} D^{v_1}u \bullet \vec{\varphi} dxdy = 0$ and $I_x^{v_2} I_y^{v_2} D^{v_1}u \bullet \vec{\varphi} = 0$, we solve, respectively:

$$\begin{aligned} \frac{\partial^{v_2} u(x,y,t)}{\partial t^{v_2}} &= -\frac{1}{4\pi^2} \\ &\quad \times \mathrm{Re}\left\{\overline{D_x^{v_1}}\varphi_x[u(x,y,t)] + \overline{D_y^{v_1}}\varphi_y[u(x,y,t)]\right\}, \end{aligned} \tag{79}$$

$$\begin{aligned} \frac{\partial^{v_3} u(x,y,t)}{\partial t^{v_3}} &= \frac{\Gamma(1+v_1)}{\Gamma(v_1)} \\ &\quad \times \left\{D_x^1\varphi_x[u(x,y,t)] + D_y^1\varphi_y[u(x,y,t)]\right\}, \end{aligned} \tag{80}$$

where $\vec{\varphi}(x, y, t) = (\varphi_x, \varphi_y) = \{\varphi_x[u(x, y, t)], \varphi_y[u(x, y, t)]\}$ and v_1, v_2, and v_3 are positive real numbers, respectively.

IV. EXPERIMENT AND ANALYSIS

Fractional calculus has been applied to the solution of a necessary condition for the fractional-order fixed boundary optimization problems in signal processing and image processing mainly because of its inherent strengths in terms of long-term memory, non-locality, and weak singularity. Fractional differential of an image can preserve the low-frequency contour feature in the smooth area, and nonlinearly keep high-frequency edge information and texture information in those areas where grey scale changes frequently, and as well as, nonlinearly enhance texture details in those areas where grey scale does not change evidently [62]–[69]. Thus, it is natural to ponder whether the fractional-order variational method based texture inpainting/denoising could nonlinearly restore/preserve the complex texture details of an image while inpainting/denoising or not.

For the convenience of implementation, the fractional-order Euler-Lagrange equation based on fractional-order Green formula is employed in the following examples. From (63), we can see that first, $\frac{\Gamma(1+v_1)}{\Gamma(v_1)}[D_x^1\varphi_x + D_y^1\varphi_y] = 0$ is the fractional-order Euler-Lagrange equation of $-I_x^{v_2} I_y^{v_2} D^{v_1}u \bullet \vec{\varphi} = 0$, which can be directly and easily implemented in spatial domain or time domain. Second, $\frac{\Gamma(1+v_1)}{\Gamma(v_1)}[D_x^1\varphi_x + D_y^1\varphi_y] = 0$ is irrelevant to the order v_2

of fractional integral $-I_x^{v_2} I_y^{v_2} D^{v_1} u \bullet \vec{\varphi} = 0$. Thus, let $v_2 = 1$ for most real applications.

A. INPAINTING BASED ON FRACTIONAL-ORDER VARIATIONAL METHOD

In this subsection, in order to take advantage of the fractional-order Euler-Lagrange equation, a fractional-order inpainting algorithm based on the fractional-order variational method is illustrated.

Example 3: Inpainting is an image restoration problem, which is the process of filling in the missing or desired image information on the unavailable domains. Different from the traditional integer-order variational method based inpainting method [22]–[29], the fractional-order differential of an image and the fraction-power norm of this fractional-order differential are used for a fractional-order variational method based texture inpainting. A fractional-order inpainting algorithm model is to minimize a fractional-order appropriate energy functional:

$$\begin{aligned} E[u|u_0] &= \underset{A\cup B}{I_x^1 I_y^1} f\left(\left|D^{v_1}u\right|^{v_2}\right) + \underset{B}{I_x^1 I_y^1} \frac{\lambda_B}{2}(u-u_0)^2 \\ &= \underset{A\cup B}{\iint} f\left(\left|D^{v_1}u\right|^{v_2}\right) dxdy + \underset{B}{\iint} \frac{\lambda_B}{2}(u-u_0)^2 dxdy, \end{aligned} \tag{81}$$

where B denotes the inpainting domain where original image is missing, A denotes the neighbourhood of B, $u(x,y)$ is an image to be inpainted, $u_0(x,y)$ is the available part of the image u on $\Omega\backslash B$ that is often noisy, Ω is an entire image domain in real plane R^2 with smooth boundary, Ω bears a rectangular shape for most real applications, $f()$ is an analytic function, E denotes a fractional-order multi-variable energy functional, $E[u|u_0]$ still means $E[u]$, but with u_0 fixed as known, v_1 and v_2 are positive real numbers, $D^{v_1} = \left(D_x^{v_1}, D_y^{v_1}\right)$ denotes the v_1-order differential operator, and $\lambda_B(x,y) = \lambda \cdot 1_{\Omega\backslash B}(x,y)$ denotes a regularization parameter. The fractional-order Neumann boundary condition of (81) is $\langle D^{v_1}u, \vec{n}\rangle = \dfrac{\partial^{v_1}u}{\partial \vec{n}^{v_1}} = 0$, where $\vec{n}$ denotes the normal to the boundary of u. It's important to note that at first, we assume that the image to be inpainted, $u(x,y)$, is spatially smooth and rich in textural details. Thus, the corresponding fractional-order regularization term is given by $\underset{A\cup B}{\iint} f\left(\left|D^{v_1}u\right|^{v_2}\right) dxdy$. Secondly, we assume that the inpainting domain is close to its neighbourhood, which means that the difference between $u(x,y)$ and $u_0(x,y)$ should be small. Thus, the penalty term $\underset{B}{\iint} \dfrac{\lambda_B}{2}(u-u_0)^2 dxdy$ is used for the fidelity, which makes the proposed model better conditioned.

Let us assume that $u(x,y)$ is the first-order extremal surface of energy functional E, $\xi(x,y) \in C_0^\infty(\Omega)$ is an admissible surface, a test function, closing to $u(x,y)$. $u(x,y)$ and $\xi(x,y)$ can be merged into a family of surfaces, $u+\alpha\xi$, where α is a small parameter. When $\alpha = 0$, the family of surfaces, $u+\alpha\xi$, converts into the first-order extremal surface, $u(x,y)$. Thus, the first-order anisotropic diffusion of (81) can be explained as the first-order dissipation process of a fractional-order multi-variable energy functional E. To achieve the first-order minimum of (81), the first-order derivative of a fractional-order energy functional on the family of surfaces, $u+\alpha\xi$, is given as (82), as shown at the bottom of this page.

At first, for the first item on the right side of (97), as shown at the bottom of this page, if the first-order differential of $f\left(\left|D^{v_1}u+\alpha D^{v_1}\xi\right|^{v_2}\right)$ with respect to α is existed, $\delta_1(\alpha)$ has a first-order extreme point, a first-order stationary point, when $\alpha = 0$. Thus, from (97), the following can be obtained:

$$\begin{aligned} &D_\alpha^1 \delta_1(\alpha)\Big|_{\alpha=0} \\ &= D_\alpha^1 \underset{A\cup B}{\iint} f\left(|\vec{\varphi}|^{v_2}\right) dxdy\Big|_{\alpha=0} \\ &= \underset{A\cup B}{\iint} D_\alpha^1 f\left(|\vec{\varphi}|^{v_2}\right) dxdy\Big|_{\alpha=0} \\ &= \underset{A\cup B}{\iint} D^1_{|\vec{\varphi}|^{v_2} f}\Big|_{\alpha=0} v_2 \left|D^{v_1}u\right|^{v_2-2} D^{v_1}u \bullet D^{v_1}\xi dxdy \\ &= 0, \end{aligned} \tag{83}$$

where with regard to a vector $\vec{\varphi} = D^{v_1}u + \alpha D^{v_1}\xi$, we have $\|\vec{\varphi}\|_2^2 = \sum_{i=1}^{2} |\varphi_i|^2 = (\vec{\varphi})^T\vec{\varphi} = \vec{\varphi} \bullet \vec{\varphi}$, where symbol $\bullet$ denotes the inner product. For the convenience of illustration, in this paper, the equivalent notations $|| = \|\|_2$ are used in an arbitrary, interchangeable manner. Equation (83) searches for the first-order extreme point of $\delta_1(\alpha)$ with respect to α. Because $\xi(x,y)$ is a test function, $D^{v_1}\xi$ is arbitrary. Therefore,

$$\begin{aligned} D_\alpha^1 \delta E\Big|_{\alpha=0} &= D_\alpha^1 \left[\delta_1(\alpha) + \delta_2(\alpha)\right]\Big|_{\alpha=0} \\ &= D_\alpha^1 \underset{A\cup B}{I_x^1 I_y^1} f\left(\left|D^{v_1}u+\alpha D^{v_1}\xi\right|^{v_2}\right)\Big|_{\alpha=0} + D_\alpha^1 \underset{B}{I_x^1 I_y^1} \frac{\lambda_B}{2}(u+\alpha\xi-u_0)^2\Big|_{\alpha=0} \\ &= D_\alpha^1 \underset{A\cup B}{\iint} f\left(\left|D^{v_1}u+\alpha D^{v_1}\xi\right|^{v_2}\right) dxdy\Big|_{\alpha=0} + D_\alpha^1 \underset{B}{\iint} \frac{\lambda_B}{2}(u+\alpha\xi-u_0)^2 dxdy\Big|_{\alpha=0} \\ &= 0. \end{aligned} \tag{82}$$

$$-\frac{\Gamma(1-v_1)}{\Gamma(-v_1)}\left[D_x^1\left(D^1_{|\vec{\varphi}|^{v_2}}f\Big|_{\alpha=0}v_2\left|D^{v_1}u\right|^{v_2-2}D_x^{v_1}u\right)+D_y^1\left(D^1_{|\vec{\varphi}|^{v_2}}f\Big|_{\alpha=0}v_2\left|D^{v_1}u\right|^{v_2-2}D_y^{v_1}u\right)\right]=0. \tag{84}$$

from (63), to enable (83) to be set up, a necessary condition can be given (84), as shown at the top of this page.

Without loss of generality, let us set $f\left(|\vec{\varphi}|^{v_2}\right)=|\vec{\varphi}|^{v_2}$. Thus, $D^1_{|\vec{\varphi}|^{v_2}}f=1$. Substituting $D^1_{|\vec{\varphi}|^{v_2}}f=1$ into (84), one can obtain:

$$-\frac{\Gamma(1-v_1)}{\Gamma(-v_1)}v_2\left[D_x^1\left(\left|D^{v_1}u\right|^{v_2-2}D_x^{v_1}u\right)+D_y^1\left(\left|D^{v_1}u\right|^{v_2-2}D_y^{v_1}u\right)\right]=0. \tag{85}$$

Secondly, for the second item on the right side of (82), the following can be obtained:

$$\begin{aligned}D_\alpha^1\delta_2(\alpha)\Big|_{\alpha=0}&=D_\alpha^1\,I_x^1I_y^1\,\frac{\lambda_{\mathrm{B}}}{2}(u+\alpha\xi-u_0)^2\Big|_{\alpha=0}\\&=I_x^1I_y^1\,D_\alpha^1\left[\frac{\lambda_{\mathrm{B}}}{2}(u+\alpha\xi-u_0)^2\right]\Big|_{\alpha=0}\\&=\iint_{\mathrm{B}}\lambda_{\mathrm{B}}(u-u_0)\xi\,dxdy\\&=0.\end{aligned} \tag{86}$$

Since $\xi(x,y)$ is a test function, the corresponding $\xi(x,y)$ is arbitrary. Therefore, according to the fundamental lemma of variation [6], [16], to enable (86) to be set up, a necessary condition can be given as:

$$\lambda_{\mathrm{B}}(u-u_0)=0. \tag{87}$$

Thus, from (85) and (87), we can derive the fractional-order Euler-Lagrange equation of $D_\alpha^1\delta E(\alpha)\big|_{\alpha=0}=0$, given as:

$$-\frac{\Gamma(1-v_1)}{\Gamma(-v_1)}v_2\left[D_x^1\left(\left|D^{v_1}u\right|^{v_2-2}D_x^{v_1}u\right)+D_y^1\left(\left|D^{v_1}u\right|^{v_2-2}D_y^{v_1}u\right)\right]+\lambda_{\mathrm{B}}(u-u_0)=0. \tag{88}$$

The solution procedure of (88) uses a parabolic equation with time as an evolution parameter (the time marching method), or equivalently, the first-order gradient descent method. Note that, we treat an image as a function of time and space, and use the time marching method to search the fractional-order steady state of (88). This means that we solve:

$$\frac{\partial u}{\partial t}=\frac{\Gamma(1-v_1)}{\Gamma(-v_1)}v_2\left[D_x^1\left(\left|D^{v_1}u\right|^{v_2-2}D_x^{v_1}u\right)+D_y^1\left(\left|D^{v_1}u\right|^{v_2-2}D_y^{v_1}u\right)\right]-\lambda_{\mathrm{B}}(u-u_0). \tag{89}$$

When $\dfrac{\partial u}{\partial t}=0$, the time marching method converges to the first-order steady state of (88). Furthermore, we must compute $\lambda_B(t)$ in (89). Let us suppose that $\iint_{\mathrm{A}}(u-u_0)dxdy=0$ and $\iint_{\mathrm{A}}(u-u_0)^2dxdy=\sigma^2$, where σ^2 is the variance of the added noise of u_0. We multiply by $(u-u_0)$ on the both sides of (88) and integrate by parts in the domain of B, the left side of (88) vanishes. Thus, the following can be obtained as (90), as shown at the top of the next page.

Equations (89) and (90), as shown at the top of the next page, should be numerically implemented. At first, let us suppose Δt denotes time interval, $n=0,1,\cdots$ denotes time (the number of iterations). Thus, $t_n=n\Delta t$. Here $t_0=0$ denotes an initial time. In (89) and (90), $u^n=u(x,y,t_n)$, and $u_0^n(x,y,t_n)=u_0^0(x,y,t_0)$. Secondly, in (79), (80), (89), and (90), the fractional-order differential operators, D^v, D_x^v, and D_y^v, of a two-dimensional signal such as digital image should be numerically implemented. Equation (1) shows that for the Grünwald-Letnikov definition of fractional calculus, the limit symbol may be removed when N is sufficiently large. Thus, the convergence rate and accuracy are improved by introducing a signal value at a non-node into the Grünwald-Letnikov definition, i.e. ${}_a^{G-L}D_x^vf(x)\cong\dfrac{x^{-v}N^v}{\Gamma(-v)}\sum_{k=0}^{N-1}\dfrac{\Gamma(k-v)}{\Gamma(k+1)}f(x+\dfrac{vx}{2N}-\dfrac{kx}{N})$. Using the Lagrange interpolation polynomial when $n=3$ points to perform the fractional-order interpolation, we can obtain the fractional-order differential operator in the eight symmetric directions [62], [68], [69]. Thus, the discrete definitions of D_x^v and D_y^v in two-dimensional space [69] are as (91) and (92), as shown at the top of the next page.

In particular, when $v=1$, the fractional-order differential operator is converted to the traditional first-order differential operator. Thirdly, in (89), according to the first-order gradient descent method, one can obtain:

$$\frac{\partial u}{\partial t}\approx\frac{u^{n+1}-u^n}{\Delta t}. \tag{93}$$

Thus, from (89), (90), and (93), the following can be obtained (94) and (95), as shown at the top of the next page, where $\sigma^{n^2}=\sum_{x,y}\left(u^n-u_0^0\right)^2$. Fourthly, the numerical implementation of the fractional-order partial differential equation should be restricted by Courant-Friedrichs-Lewy (CFL) condition [122]. Finally, it may be considered that $|D^{v_1}u^n|=0$ during the numerical iteration computation of (94) and (95). To enable (94) and (95) to be implemented, if $|D^{v_1}u^n|\le\varepsilon$, let us set $|D^{v_1}u^n|=\varepsilon$, where ε is a small positive constant. Without loss of generality, in the following experiments, let us set $\varepsilon=10^{-5}$.

In order to illustrate the capability of restoring the edges and textural details of the fractional-order inpainting algorithm based on the fractional-order variational method, it was analyzed by considering the integer-order inpainting algorithm based on the classic integer-order variational method [21]–[29] vis-à-vis the proposed fractional-order inpainting algorithm and a suitable texture image i.e. a hair image. We artificially damaged the original hair image at random

$$\lambda_{\mathrm{B}}(t) = \frac{\Gamma(1-v_1)}{\sigma^2\Gamma(-v_1)} v_2 \iint_{\mathrm{A}} \left[D_x^1 \left(\left| D^{v_1} u \right|^{v_2-2} D_x^{v_1} u \right) + D_y^1 \left(\left| D^{v_1} u \right|^{v_2-2} D_y^{v_1} u \right) \right] (u - u_0) dxdy. \tag{90}$$

$$\begin{aligned} D_x^v u(x,y,t) \approx & \left(\frac{v}{4} + \frac{v^2}{8}\right) u(x+1,y,t) + \left(1 - \frac{v^2}{2} - \frac{v^3}{8}\right) u(x,y,t) \\ & + \frac{1}{\Gamma(-v)} \sum_{k=1}^{n-2} \left[\frac{\Gamma(k-v+1)}{(k+1)!} \cdot \left(\frac{v}{4} + \frac{v^2}{8}\right) + \frac{\Gamma(k-v)}{k!} \cdot \left(1 - \frac{v^2}{4}\right) + \frac{\Gamma(k-v-1)}{(k-1)!} \cdot \left(-\frac{v}{4} + \frac{v^2}{8}\right) \right] u(x-k,y,t) \\ & + \left[\frac{\Gamma(n-v-1)}{(n-1)!\Gamma(-v)} \cdot \left(1 - \frac{v^2}{4}\right) + \frac{\Gamma(n-v-2)}{(n-2)!\Gamma(-v)} \cdot \left(-\frac{v}{4} + \frac{v^2}{8}\right) \right] u(x-n+1,y,t) \\ & + \frac{\Gamma(n-v-1)}{(n-1)!\Gamma(-v)} \cdot \left(-\frac{v}{4} + \frac{v^2}{8}\right) u(x-n,y,t), \end{aligned} \tag{91}$$

$$\begin{aligned} D_y^v u(x,y,t) \approx & \left(\frac{v}{4} + \frac{v^2}{8}\right) u(x,y+1,t) + \left(1 - \frac{v^2}{2} - \frac{v^3}{8}\right) u(x,y,t) \\ & + \frac{1}{\Gamma(-v)} \sum_{k=1}^{n-2} \left[\frac{\Gamma(k-v+1)}{(k+1)!} \cdot \left(\frac{v}{4} + \frac{v^2}{8}\right) + \frac{\Gamma(k-v)}{k!} \cdot \left(1 - \frac{v^2}{4}\right) + \frac{\Gamma(k-v-1)}{(k-1)!} \cdot \left(-\frac{v}{4} + \frac{v^2}{8}\right) \right] u(x,y-k,t) \\ & + \left[\frac{\Gamma(n-v-1)}{(n-1)!\Gamma(-v)} \cdot \left(1 - \frac{v^2}{4}\right) + \frac{\Gamma(n-v-2)}{(n-2)!\Gamma(-v)} \cdot \left(-\frac{v}{4} + \frac{v^2}{8}\right) \right] u(x,y-n+1,t) \\ & + \frac{\Gamma(n-v-1)}{(n-1)!\Gamma(-v)} \cdot \left(-\frac{v}{4} + \frac{v^2}{8}\right) u(x,y-n,t), \end{aligned} \tag{92}$$

$$u^{n+1} = \frac{\Gamma(1-v_1)}{\Gamma(-v_1)} v_2 \left[D_x^1 \left(\left| D^{v_1} u^n \right|^{v_2-2} D_x^{v_1} u^n \right) + D_y^1 \left(\left| D^{v_1} u^n \right|^{v_2-2} D_y^{v_1} u^n \right) \right] \Delta t - \lambda_{\mathrm{B}}^n \Delta t u_0^n + (1 + \lambda_{\mathrm{B}}^n \Delta t) u^n, \tag{94}$$

$$\lambda_{\mathrm{B}}^n = \frac{\Gamma(1-v_1)}{\sigma^{n^2}\Gamma(-v_1)} v_2 \sum_{x,y} \left[D_x^1 \left(\left| D^{v_1} u^n \right|^{v_2-2} D_x^{v_1} u^n \right) + D_y^1 \left(\left| D^{v_1} u^n \right|^{v_2-2} D_y^{v_1} u^n \right) \right] (u^n - u^0), \tag{95}$$

and used this damaged image as the test image. No *a priori* knowledge regarding the characteristics of the original hair image is either known or required. We set $v_1 = 2.25$ and $v_2 = 2.5$ in (94) and (95). Suppose we set the same parameters, the time interval $\Delta t = 0.0001$, the number of iterations $n = 150$, for both the fractional-order inpainting algorithm and the integer-order one in this simulation experiment. Thus, the results of the comparative inpainting experiments for the hair image are shown in Fig. 3.

To consider the visual effects for the purpose of comparison, from Fig. 3 (a), (b), (e), (f), (g), and (h), we can see that the capability of the integer-order inpainting algorithm based on the integer-order variational method to restore the edges and textural details is worse than that of the fractional-order inpainting algorithm based on the fractional-order variational method. In particular, the extent to which the integer-order inpainting algorithm is able to restore the local edges and textural details is relatively weaker than that of the fractional-order inpainting algorithm. The integer-order inpainting algorithm tends to uniformly compensate the damaged image if there are rich local edges and textural details, often resulting in a blocky structure appearance of the output image. In comparison, the result of restoring the edges and textural details of the fractional-order inpainting algorithm is relatively clearer than that of the integer-order inpainting algorithm. The inpainted image regions of the integer-order inpainting algorithm appear relatively smoother than those produced by the fractional-order inpainting algorithm.

Next, with the objective of performing a quantitative analysis, we obtained the peak signal-to-noise ratio (PSNR) between the inpainted image and the original image to evaluate the inpainting effects of each competing algorithm under consideration. The PSNR is defined via the mean squared error (MSE). Given a noise-free $m \times n$ monochrome image I and its noisy approximated image K, the MSE can be defined as $MSE = \frac{1}{mn} \sum_{x=0}^{m-1} \sum_{y=0}^{n-1} [I(x,y) - K(x,y)]^2$. The PSNR (in dB) can be defined as $PSNR = 10 \cdot \log_{10}(MAX_I/MSE)$, where, MAX_I is the maximum possible pixel value of the image I. The PSNR of the integer-order inpainting algorithm and that of the fractional-order inpainting algorithm are 16.3560 and 19.8275, respectively. The PSNR of the integer-order inpainting algorithm is much smaller than that of the fractional-order inpainting algorithm, which shows that the high-frequency edges and textural details of the inpainted image of the integer-order inpainting algorithm is sharply diffused and smoothed. This, in turn, indicates that the

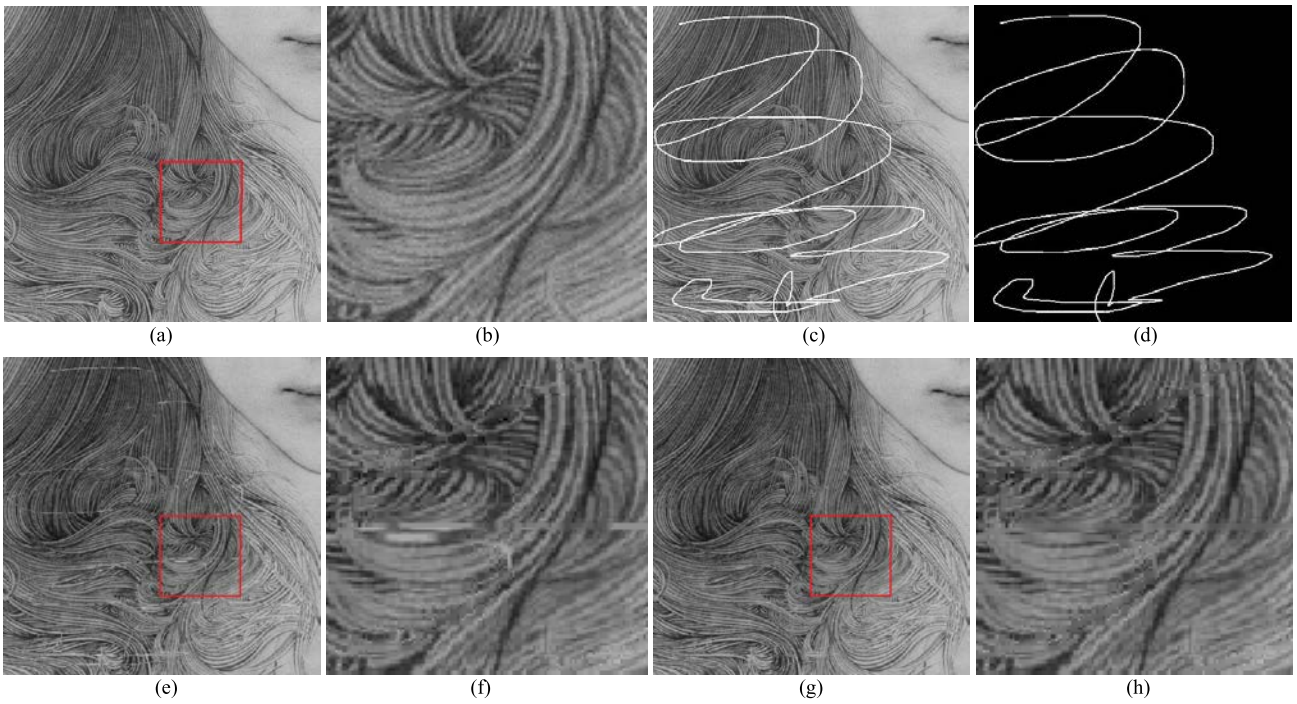

FIGURE 3. Comparative inpainting experiments on a hair image. (a) Original hair image, (b) Enlarged detail of lower right 1/16 of (a), (c) Damaged hair image, (d) Template of inpainting, (e) Integer-order inpainting algorithm, (f) Enlarged detail of lower right 1/16 of (e), (g) Fractional-order inpainting algorithm, (h) Enlarged detail of lower right 1/16 of (g).

structural similarity of the edges and textural details between its corresponding inpainted image and the original image is weaker than that of the fractional-order inpainting algorithm. The capability of restoring the edges and textural details of the fractional-order inpainting algorithm is obviously superior to that of the integer-order inpainting algorithm, especially for images rich in textural detail.

Moreover, in order to extend our analysis of the capability of the fractional-order inpainting algorithm to restore edges and textural details, we chose another suitable texture image i.e. a wood grain image to further illustrate. We also randomly damaged the original wood grain image and used this damaged image as the test image. No *a priori* knowledge regarding the characteristics of the original wood grain image is either known or required. We still set $v_1 = 2.25$ and $v_2 = 2.5$ in (94) and (95). Suppose we set the same parameters, the time interval $\Delta t = 0.0001$, the number of iterations $n = 90$, for both the fractional-order inpainting algorithm and the integer-order one in this simulation experiment. Thus, the results of the comparative inpainting experiments for the wood grain image are shown in Fig. 4.

From Fig. 4 (a), (b), (e), (f), (g), and (h), we can see that the result of restoring the edges and textural details of the fractional-order inpainting algorithm is relatively clearer than that of the integer-order inpainting algorithm. The inpainted image regions of the integer-order inpainting algorithm appear relatively smoother than those produced by the fractional-order inpainting algorithm. Next, the PSNR of the integer-order inpainting algorithm and that of the fractional-order inpainting algorithm are 15.4562 and 16.5723, respectively. The capability of restoring the edges and textural details of the fractional-order inpainting algorithm is obviously superior to that of the integer-order inpainting algorithm, especially for images rich in textural detail.

In addition, as the next experimental step, we then selected another suitable texture image i.e. a moonscape image for the purpose of implementing comparative experiments. We also stochastically damaged the original moonscape image and used this damaged image as the test image. No *a priori* knowledge regarding the characteristics of the original moonscape image is either known or required. We still set $v_1 = 2.25$ and $v_2 = 2.5$ in (94) and (95). Suppose we set the same parameters, the time interval $\Delta t = 0.0001$, the number of iterations $n = 150$, for both the fractional-order inpainting algorithm and the integer-order one in this simulation experiment. Thus, the results of the comparative inpainting experiments for the moonscape image are shown in Fig. 5.

From Fig. 5 (a), (b), (e), (f), (g), and (h), we can see that the result of restoring the edges and textural details of the fractional-order inpainting algorithm is relatively clearer than that of the integer-order inpainting algorithm. The inpainted image regions of the integer-order inpainting algorithm appear relatively smoother than those produced by the fractional-order inpainting algorithm. Next, the PSNR of the integer-order inpainting algorithm and that of the fractional-order inpainting algorithm are 21.7132 and 23.0138, respectively. The capability of restoring the edges and textural

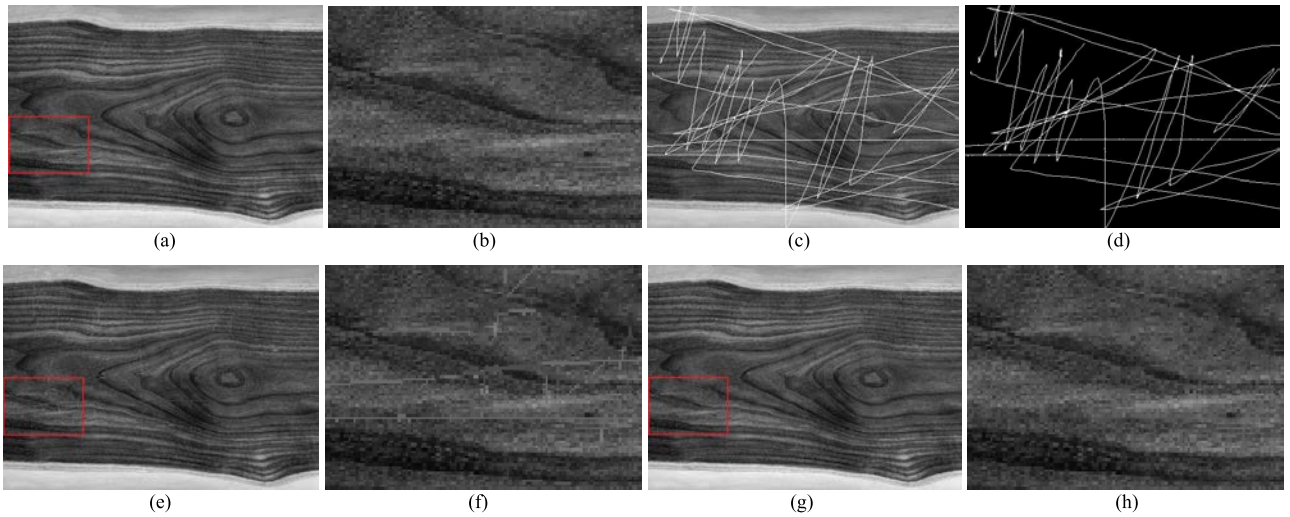

FIGURE 4. Comparative inpainting experiments on a wood grain image. (a) Original wood grain image, (b) Enlarged detail of lower left 1/16 of (a), (c) Damaged wood grain image, (d) Template of inpainting, (e) Integer-order inpainting algorithm, (f) Enlarged detail of lower left 1/16 of (e), (g) Fractional-order inpainting algorithm, (h) Enlarged detail of lower left 1/16 of (g).

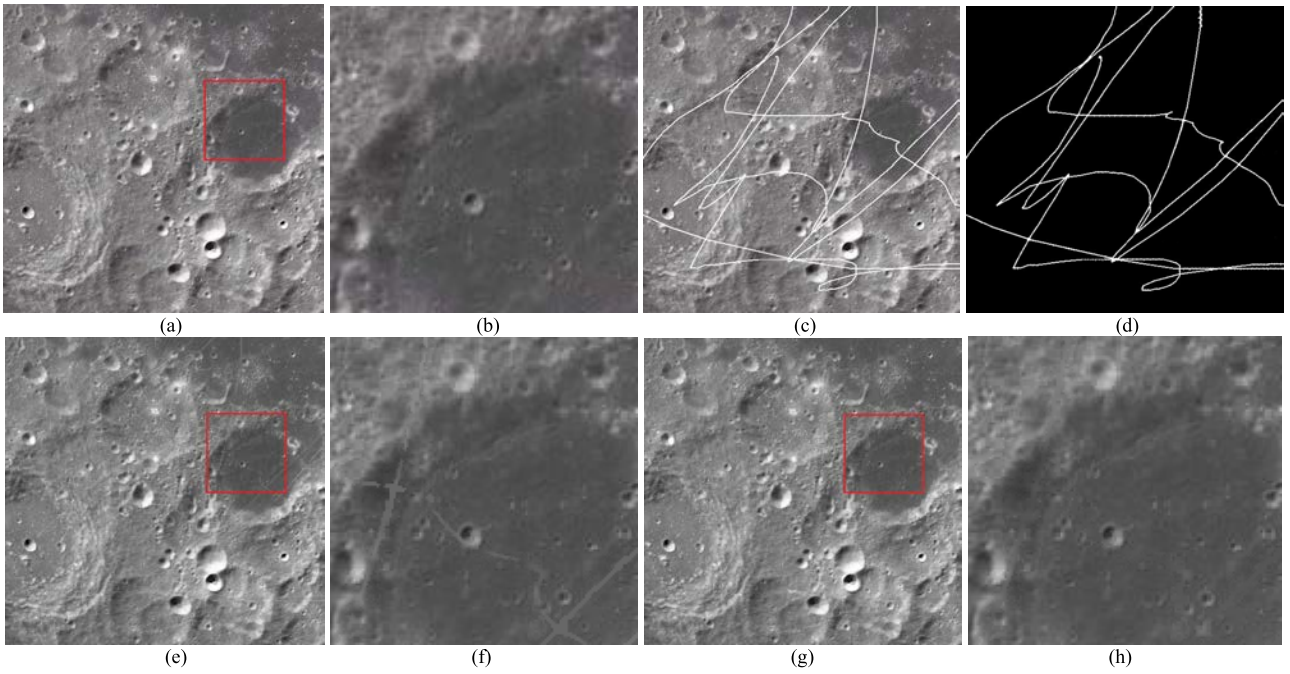

FIGURE 5. Comparative inpainting experiments on a moonscape image. (a) Original moonscape image, (b) Enlarged detail of higher right 1/16 of (a), (c) Damaged moonscape image, (d) Template of inpainting, (e) Integer-order inpainting algorithm, (f) Enlarged detail of higher right 1/16 of (e), (g) Fractional-order inpainting algorithm, (h) Enlarged detail of higher right 1/16 of (g).

details of the fractional-order inpainting algorithm is obviously superior to that of the integer-order inpainting algorithm, especially for images rich in textural detail.

B. IMAGE DENOISING BASED ON FRACTIONAL-ORDER VARIATIONAL METHOD

In this subsection, in order to take advantage of the fractional-order Euler-Lagrange equation, a fractional-order denoising algorithm based on the fractional-order variational method is illustrated.

Example 4: Image denoising is another image restoration problem. Different from the traditional integer-order variational method based image denoising method [17]–[21], the fractional-order differential of an image, the fraction-power norm of this fractional-order differential, and the fractional-order extreme point of their energy functional are used for the fractional-order variational method based

$$\begin{aligned} D_\alpha^{v_3}\delta E &= D_\alpha^{v_3}\left[\delta_1(\alpha)+\delta_2(\alpha)\right] \\ &= D_\alpha^{v_3}\underset{\Omega}{I_x^1 I_y^1} f\left[\left|D^{v_1}u+(\alpha-1)D^{v_1}\xi\right|^{v_2}\right]+D_\alpha^{v_3}\underset{\Omega}{I_x^1 I_y^1}\lambda\left[u+(\alpha-1)\xi-u_0\right]u_0 \\ &= D_\alpha^{v_3}\iint\limits_{\Omega} f\left[\left|D^{v_1}u+(\alpha-1)D^{v_1}\xi\right|^{v_2}\right]dxdy+D_\alpha^{v_3}\lambda\iint\limits_{\Omega}\left[u+(\alpha-1)\xi-u_0\right]u_0 dxdy \\ &= 0, \end{aligned} \tag{97}$$

image denoising. A fractional-order denoising algorithm is to minimize a fractional-order appropriate energy functional:

$$\begin{aligned} E[u] &= \underset{\Omega}{I_x^1 I_y^1} f\left(\left|D^{v_1}u\right|^{v_2}\right)+\underset{\Omega}{I_x^1 I_y^1}\lambda(u-u_0)u_0 \\ &= \iint\limits_{\Omega} f\left(\left|D^{v_1}u\right|^{v_2}\right)dxdy+\lambda\iint\limits_{\Omega}(u-u_0)u_0 dxdy, \end{aligned} \tag{96}$$

where u denotes a clean image, u_0 denotes a noisy image, λ denotes a regularization parameter, Ω is an the entire image domain in real plane R^2 with smooth boundary, Ω bears a rectangular shape for most real applications, E denotes a fractional-order multi-variable energy functional, $f()$ is an analytic function, v_1 and v_2 are positive real numbers, $D^{v_1}=\left(D_x^{v_1},D_y^{v_1}\right)$ denotes the v_1-order differential operator, and λ denotes a regularization parameter. The fractional-order Neumann boundary condition of (96) is $\langle D^{v_1}u,\vec{\boldsymbol{n}}\rangle=\frac{\partial^{v_1}u}{\partial\vec{\boldsymbol{n}}^{v_1}}=0$, where $\vec{\boldsymbol{n}}$ denotes the normal to the boundary of u. It's important to note that at first, we assume that the clean image, $u(x,y)$, is spatially smooth and rich in textural details. Thus, the corresponding fractional-order regularization term is given by $\iint_{\Omega} f\left(\left|D^{v_1}u\right|^{v_2}\right)dxdy$. Secondly, we assume that the clean image is close to the noisy image, which means that the difference between $u(x,y)$ and $u_0(x,y)$ should be small. Thus, the penalty term $\lambda\iint_{\Omega}(u-u_0)u_0 dxdy$ is used for the fidelity, which makes the proposed model better conditioned. In order to avoid incomplete beta function being not set up, the fidelity term in (96) is set to $\lambda\iint_{\Omega}(u-u_0)u_0 dxdy$, rather than $\lambda\iint_{\Omega}(u-u_0)^2 dxdy$, where $\lambda\iint_{\Omega}(u-u_0)u_0 dxdy$ is a cross energy between $(u-u_0)$ and u_0.

Let us assume that $u(x,y)$ is the fractional-order extremal surface of a fractional-order energy functional E, $\xi(x,y)\in C_0^\infty(\Omega)$ is an admissible surface, a test function, closing to $u(x,y)$. Then, $u(x,y)$ and $\xi(x,y)$ can be merged into a family of surfaces, $u+(\alpha-1)\xi$, where α is a small parameter. When $\alpha=1$, the family of surfaces, $u+(\alpha-1)\xi$, converts into the fractional-order extremal surface, $u(x,y)$. Thus, the fractional-order anisotropic diffusion of (96) can be explained as the fractional-order dissipation process of a fractional-order multi-variable energy functional E. To achieve the fractional-order minimum of (96), the fractional-order derivative of a fractional-order energy functional on the family of surfaces, $u+(\alpha-1)\xi$, is given (97), as shown at the top of this page, where v_3 is a positive real number.

At first, for the first item on the right side of (97), if the v_3-order differential of $f\left[\left|D^{v_1}u+(\alpha-1)D^{v_1}\xi\right|^{v_2}\right]$ with respect to α is existed, $\delta_1(\alpha)$ has a v_3-order extreme point, a v_3-order stationary point, when $\alpha=1$. Thus, from (97), the following can be obtained:

$$\begin{aligned} D_\alpha^{v_3}\delta_1(\alpha)\big|_{\alpha=1} &= \frac{\partial^{v_3}}{\partial\alpha^{v_3}}\iint\limits_{\Omega} f\left(|\vec{\boldsymbol{\varphi}}|^{v_2}\right)dxdy\Bigg|_{\alpha=1} \\ &= \iint\limits_{\Omega}\frac{\partial^{v_3}}{\partial\alpha^{v_3}} f\left(|\vec{\boldsymbol{\varphi}}|^{v_2}\right)dxdy\Bigg|_{\alpha=1} \\ &= 0, \end{aligned} \tag{98}$$

where with regard to a vector $\vec{\boldsymbol{\varphi}}=D^{v_1}u+(\alpha-1)D^{v_1}\xi$, we have $\|\vec{\boldsymbol{\varphi}}\|_2^2=\sum_{i=1}^{2}|\varphi_i|^2=(\vec{\boldsymbol{\varphi}})^T\vec{\boldsymbol{\varphi}}=\vec{\boldsymbol{\varphi}}\bullet\vec{\boldsymbol{\varphi}}$, where symbol $\bullet$ denotes the inner product. For the convenience of illustration, in this paper, the equivalent notations $||=\|\|_2$ are used in an arbitrary, interchangeable manner. Equation (98) searches for the v_3-order extreme point of $\delta_1(\alpha)$ with respect to α. Further, provided v is a fraction, when $n>v$, $\binom{v}{n}=\frac{\Gamma(1+v)}{\Gamma(1-n+v)\Gamma(1+n)}=\frac{(-1)^n\Gamma(n-v)}{\Gamma(-v)\Gamma(1+n)}\neq 0$. Thus, from (57) and Faà di Bruno's formula, it follows that (99), as shown at the top of the previous page, where ρ is an arbitrary constant and $g(\alpha)=|\vec{\boldsymbol{\varphi}}|^{v_2}$. On the right side of (99), the item of $n=0$ is separated from summation symbol $\sum_{n=0}^{\infty}$. Equation (99) shows that the fractional derivative of a composite function is equal to an infinite sum, in which P_k satisfies:

$$\begin{cases}\sum\limits_{k=1}^{n} kP_k=n \\ \sum\limits_{k=1}^{n} P_k=m.\end{cases} \tag{100}$$

The third summation symbol $\sum$ in (99) denotes the sum up of $\left\{\prod_{k=1}^{n}\frac{1}{P_k!}\left[\frac{D_{\alpha-\rho}^{k}g}{k!}\right]^{P_k}\right\}\Big|_{m=1\to n}$ corresponding to the whole combination of $P_k|_{m=1\to n}$ that satisfies (100). Thus, substituting (99) into (98), one can obtain (101), as shown at the top of the next page.

In order to simplify the calculation, without loss of generality, let us suppose that $f(\eta)=\eta$. Thus, according to

$$D^{v}_{\alpha-\rho}f\left[g\left(\alpha\right)\right]=\frac{\left(\alpha-\rho\right)^{-v}}{\Gamma\left(1-v\right)}f+\sum_{n=1}^{\infty}\binom{v}{n}\frac{\left(\alpha-\rho\right)^{n-v}}{\Gamma\left(n-v+1\right)}n!\sum_{m=1}^{n}D^{m}_{g}f\sum\prod_{k=1}^{n}\frac{1}{P_k!}\left[\frac{D^{k}_{\alpha-\rho}g}{k!}\right]^{P_k}, \tag{99}$$

$$\begin{aligned}&\iint_{\Omega}\frac{\partial^{v_3}}{\partial\alpha^{v_3}}f\left(\left|\vec{\boldsymbol{\varphi}}\right|^{v_2}\right)dxdy\Big|_{\alpha=1}\\&=\iint_{\Omega}\frac{\alpha^{-v_3}f\left(\left|\vec{\boldsymbol{\varphi}}\right|^{v_2}\right)}{\Gamma\left(1-v_3\right)}+\sum_{n=1}^{\infty}\binom{v_3}{n}\frac{\alpha^{n-v_3}}{\Gamma\left(n-v_3+1\right)}n!\sum_{m=1}^{n}D^{m}_{\left|\vec{\boldsymbol{\varphi}}\right|^{v_2}}f\sum\prod_{k=1}^{n}\frac{1}{P_k!}\left[\frac{D^{k}_{\alpha}\left(\left|\vec{\boldsymbol{\varphi}}\right|^{v_2}\right)}{k!}\right]^{P_k}dxdy\Big|_{\alpha=1}\\&=\iint_{\Omega}\frac{f\left(\left|D^{v_1}u\right|^{v_2}\right)}{\Gamma\left(1-v_3\right)}+\sum_{n=1}^{\infty}\frac{\left(-1\right)^{n}\Gamma\left(n-v_3\right)}{\Gamma\left(-v_3\right)\Gamma\left(n-v_3+1\right)}\sum_{m=1}^{n}D^{m}_{\left|\vec{\boldsymbol{\varphi}}\right|^{v_2}}f\Big|_{\alpha=1}\sum\prod_{k=1}^{n}\frac{1}{P_k!}\left[\frac{D^{k}_{\alpha}\left(\left|\vec{\boldsymbol{\varphi}}\right|^{v_2}\right)\big|_{\alpha=1}}{k!}\right]^{P_k}dxdy\\&=0.\end{aligned} \tag{101}$$

$$\iint_{\Omega}\frac{\left|D^{v_1}u\right|^{v_2}}{\Gamma\left(1-v_3\right)}+\sum_{n=1}^{\infty}\frac{\left(-1\right)^{n}\Gamma\left(n-v_3\right)}{\Gamma\left(-v_3\right)\Gamma\left(n-v_3+1\right)}\left\{\prod_{k=1}^{n}\frac{1}{P_k!}\left[\frac{D^{k}_{\alpha}\left(\left|\vec{\boldsymbol{\varphi}}\right|^{v_2}\right)\big|_{\alpha=1}}{k!}\right]^{P_k}\right\}_{m=1}dxdy=0. \tag{102}$$

properties of the integer-order calculus, $D^{1}_{\eta}f\left(\eta\right)=1$ and $D^{m}_{\eta}f\left(\eta\right)\overset{m\geq 2}{\equiv}0$. Therefore, (101) can be simplified as (102), as shown at the top of this page.

In addition, from (100), we can see that if $m=1$, P_k satisfies $P_n=1$ and $P_1=P_2=\cdots=P_{n-1}=0$. Thus, (102) can be can be further simplified as:

$$\iint_{\Omega}\frac{\left|D^{v_1}u\right|^{v_2}}{\Gamma\left(1-v_3\right)}+\sum_{n=1}^{\infty}\frac{\left(-1\right)^{n}\Gamma\left(n-v_3\right)}{\Gamma\left(-v_3\right)\Gamma\left(n-v_3+1\right)}\frac{D^{n}_{\alpha}\left(\left|\vec{\boldsymbol{\varphi}}\right|^{v_2}\right)\big|_{\alpha=1}}{n!}dxdy=0. \tag{103}$$

Further, the expression of $D^{n}_{\alpha}\left(\left|\vec{\boldsymbol{\varphi}}\right|^{v_2}\right)\big|_{\alpha=1}$ when n is an odd number ($n=2k+1,\quad k=0,1,2,3\cdots$) is different from that of $D^{n}_{\alpha}\left(\left|\vec{\boldsymbol{\varphi}}\right|^{v_2}\right)\big|_{\alpha=1}$ when n is an even number ($n=2k,\quad k=1,2,3\cdots$), which can be given as, respectively:

$$\begin{aligned}D^{n}_{\alpha}\left(\left|\vec{\boldsymbol{\varphi}}\right|^{v_2}\right)\Big|^{n=2k+1}_{\alpha=1}&=\prod_{\tau=1}^{n}\left(v_2-\tau+1\right)\left|D^{v_1}u\right|^{v_2-n-1}\\&\quad\times\left|D^{v_1}\xi\right|^{n-1}\left(D^{v_1}\xi\right)\bullet\left(D^{v_1}u\right),\end{aligned} \tag{104}$$

$$D^{n}_{\alpha}\left(\left|\vec{\boldsymbol{\varphi}}\right|^{v_2}\right)\Big|^{n=2k}_{\alpha=1}=\prod_{\tau=1}^{n}\left(v_2-\tau+1\right)\left|D^{v_1}u\right|^{v_2-n}\left|D^{v_1}\xi\right|^{n}. \tag{105}$$

Then, substitution of (104) and (105) into (103) results in (106), as shown at the top of the next page, where we set $\prod_{\tau=1}^{n}\left(v_2-\tau+1\right)\overset{n=0}{=}1$. Because $\xi(x,y)$ is a test function, $|D^{v_1}\xi|^{2k}$ and $D^{v_1}\xi$ are arbitrary. From (63), we can derive that $\frac{\Gamma(1+v_1)}{\Gamma(v_1)}[D^{1}_{x}\varphi_x+D^{1}_{y}\varphi_y]=0$ is the fractional-order Euler-Lagrange formula of $-\iint_{\Omega}D^{v_1}u\bullet\vec{\boldsymbol{\varphi}}dxdy=0$, where $u(x,y)$ denotes an arbitrary scalar function and $\vec{\boldsymbol{\varphi}}=\left(\varphi_x,\varphi_y\right)$ denotes a vector function. Therefore, according to the fractional-order Euler-Lagrange formula and the fundamental lemma of variation [6], [16], to enable (106) to be set up, a corresponding necessary condition can be given (107), as shown at the top of the next page, where we set $\prod_{\tau=1}^{n}\left(v_2-\tau+1\right)\overset{n=0}{=}1$.

Secondly, for the second item on the right side of (97), the following can be obtained (108), as shown at the top of the next page.

Since $\xi(x,y)$ is a test function, the corresponding $[\Gamma\left(2-v_3\right)\left(u-u_0-\xi\right)+\Gamma\left(1-v_3\right)\xi]$ is arbitrary. Therefore, according to the fundamental lemma of variation [6], [16], to enable (108) to be set up, a necessary condition can be given as:

$$\frac{\lambda u_0}{\Gamma(1-v_3)\Gamma(2-v_3)}=0. \tag{109}$$

Thus, from (107) and (109), we can derive the fractional-order Euler-Lagrange equation of $D^{v_3}_{\alpha}\delta E\left(\alpha\right)\big|_{\alpha=1}=0$, given (110), as shown at the top of the next page.

The solution procedure of (110) uses a parabolic equation with time as an evolution parameter (the time marching method), or equivalently, the fractional-order gradient descent method [73]. Note that, we treat an image as a function of time and space, and use the time marching method to search the fractional-order steady state of (110). This means that we solve (111), as shown at the top of the next page, where we set $\prod_{\tau=1}^{n}\left(v_2-\tau+1\right)\overset{n=0}{=}1$. When $\frac{\partial^{v_3}u}{\partial t^{v_3}}=0$, the time marching method converges to the fractional-order steady state of (110). Furthermore, we must compute $\lambda\left(t\right)$ in (111). Let us suppose that $\iint_{\Omega}\left(u-u_0\right)dxdy=0$

$$\iint_{\Omega}\sum_{k=0}^{\infty}\frac{\prod_{\tau=1}^{2k}(v_2-\tau+1)\left|D^{v_1}u\right|^{v_2-2k-2}\left|D^{v_1}\xi\right|^{2k}}{\Gamma(-v_3)(2k)!}\left(D^{v_1}u\right)\bullet D^{v_1}\left[\frac{\Gamma(2k-v_3)}{\Gamma(2k-v_3+1)}u-\frac{(v_2-2k)\Gamma(2k-v_3+1)}{(2k+1)\Gamma(2k-v_3+2)}\xi\right]dxdy$$
$$=\iint_{\Omega}\sum_{k=0}^{\infty}\frac{\prod_{\tau=1}^{2k}(v_2-\tau+1)}{(2k)!}\left\{\frac{\Gamma(2k-v_3)\left|D^{v_1}u\right|^{v_2-2k}}{\Gamma(-v_3)\Gamma(2k-v_3+1)}\left|D^{v_1}\xi\right|^{2k}-\frac{(v_2-2k)\Gamma(2k-v_3+1)\left|D^{v_1}u\right|^{v_2-2k-2}}{(2k+1)\Gamma(-v_3)\Gamma(2k-v_3+2)}\right.$$
$$\left.\times\left[\left(D^{v_1}u\right)\bullet\left|D^{v_1}\xi\right|^{2k}\left(D^{v_1}\xi\right)\right]\right\}dxdy$$
$$=0, \tag{106}$$

$$\sum_{k=0}^{\infty}\frac{\prod_{\tau=1}^{2k}(v_2-\tau+1)}{(2k)!}\left\{\frac{\Gamma(2k-v_3)\left|D^{v_1}u\right|^{v_2-2k}}{\Gamma(-v_3)\Gamma(2k-v_3+1)}+\frac{(v_2-2k)\Gamma(1+v_1)\Gamma(2k-v_3+1)\left|D^{v_1}u\right|^{v_2-2k-2}}{(2k+1)\Gamma(v_1)\Gamma(-v_3)\Gamma(2k-v_3+2)}\right.$$
$$\left.\times\left[D_x^1\left(D_x^{v_1}u\right)+D_y^1\left(D_y^{v_1}u\right)\right]\right\}=0, \tag{107}$$

$$D_{\alpha}^{v_3}\delta_2(\alpha)\big|_{\alpha=1}=D_{\alpha}^{v_3}I_x^1I_y^1\lambda\left[u+(\alpha-1)\xi-u_0\right]u_0\Big|_{\alpha=1}$$
$$=\iint_{\Omega}\frac{\lambda u_0}{\Gamma(1-v_3)\Gamma(2-v_3)}\left[\Gamma(2-v_3)(u-u_0-\xi)+\Gamma(1-v_3)\xi\right]dxdy$$
$$=0. \tag{108}$$

$$\sum_{k=0}^{\infty}\frac{\prod_{\tau=1}^{2k}(v_2-\tau+1)}{(2k)!}\left\{\frac{\Gamma(2k-v_3)\left|D^{v_1}u\right|^{v_2-2k}}{\Gamma(-v_3)\Gamma(2k-v_3+1)}+\frac{(v_2-2k)\Gamma(1+v_1)\Gamma(2k-v_3+1)\left|D^{v_1}u\right|^{v_2-2k-2}}{(2k+1)\Gamma(v_1)\Gamma(-v_3)\Gamma(2k-v_3+2)}\right.$$
$$\left.\times\left[D_x^1\left(D_x^{v_1}u\right)+D_y^1\left(D_y^{v_1}u\right)\right]\right\}+\frac{\lambda u_0}{\Gamma(1-v_3)\Gamma(2-v_3)}=0. \tag{110}$$

$$\frac{\partial^{v_3}u}{\partial t^{v_3}}=-\sum_{k=0}^{\infty}\frac{\prod_{\tau=1}^{2k}(v_2-\tau+1)}{(2k)!}\left\{\frac{\Gamma(2k-v_3)\left|D^{v_1}u\right|^{v_2-2k}}{\Gamma(-v_3)\Gamma(2k-v_3+1)}+\frac{(v_2-2k)\Gamma(1+v_1)\Gamma(2k-v_3+1)\left|D^{v_1}u\right|^{v_2-2k-2}}{(2k+1)\Gamma(v_1)\Gamma(-v_3)\Gamma(2k-v_3+2)}\right.$$
$$\left.\times\left[D_x^1\left(D_x^{v_1}u\right)+D_y^1\left(D_y^{v_1}u\right)\right]\right\}-\frac{\lambda u_0}{\Gamma(1-v_3)\Gamma(2-v_3)}, \tag{111}$$

$$\lambda=\frac{-\Gamma(1-v_3)\Gamma(2-v_3)}{\sigma^2}\iint_{\Omega}\sum_{k=0}^{\infty}\frac{\prod_{\tau=1}^{2k}(v_2-\tau+1)}{(2k)!}\left\{\frac{\Gamma(2k-v_3)\left|D^{v_1}u\right|^{v_2-2k}}{\Gamma(-v_3)\Gamma(2k-v_3+1)}\right.$$
$$\left.+\frac{(v_2-2k)\Gamma(1+v_1)\Gamma(2k-v_3+1)\left|D^{v_1}u\right|^{v_2-2k-2}}{(2k+1)\Gamma(v_1)\Gamma(-v_3)\Gamma(2k-v_3+2)}\left[D_x^1\left(D_x^{v_1}u\right)+D_y^1\left(D_y^{v_1}u\right)\right]\right\}\frac{(u-u_0)^2}{u_0}dxdy. \tag{112}$$

and $\iint_{\Omega}(u-u_0)^2dxdy=\sigma^2$, where σ^2 is the variance of the added noise of u_0. We multiply by $(u-u_0)^2/u_0$ on the both sides of (110) and integrate by parts in the domain of Ω, the left side of (110) vanishes. Thus, the following can be obtained (112), as shown at the top of this page.

Equations (111) and (112) should be numerically implemented. At first, in (111), according to the fractional-order gradient descent method [73], one can obtain:

$$\frac{\partial^{v_3}u}{\partial t^{v_3}}=\Delta t^{-v_3}\left[u^{n+1}-u^n+\frac{2\mu\eta}{\Gamma(3-v_3)}(u^n-u^{v_3*})^2(u^n)^{-v_3}\right], \tag{113}$$

$$u^{n+1} = I\left(u^n\right)\Delta t^{v_3} - \frac{\lambda^n \Delta t^{v_3}}{\Gamma(1-v_3)\Gamma(2-v_3)}u_0^n + u^n - \frac{2\mu}{\Gamma(3-v_3)}\left(u^{n-1}-u^n\right)^2\left(u^n\right)^{-v_3}, \tag{114}$$

$$\lambda^n = \frac{\Gamma(1-v_3)\Gamma(2-v_3)}{\sigma^{n^2}}\sum_{(x,y)\in\Omega} I(u^n)\frac{\left(u^n-u_0^n\right)^2}{u_0^n}, \tag{115}$$

$$I\left(u^n\right) = -\sum_{k=0}^{1}\frac{\prod_{\tau=1}^{2k}(v_2-\tau+1)}{(2k)!}\left\{\frac{\Gamma\left(2k-v_3\right)\left|D^{v_1}u^n\right|^{v_2-2k}}{\Gamma\left(-v_3\right)\Gamma\left(2k-v_3+1\right)} + \frac{\left(v_2-2k\right)\Gamma\left(1+v_1\right)\Gamma\left(2k-v_3+1\right)\left|D^{v_1}u^n\right|^{v_2-2k-2}}{(2k+1)\Gamma\left(v_1\right)\Gamma\left(-v_3\right)\Gamma\left(2k-v_3+2\right)} \times\left[D_x^1\left(D_x^{v_1}u^n\right)+D_y^1\left(D_y^{v_1}u^n\right)\right]\right\}, \tag{116}$$

where u^{v_3*} is the v_3-order optimal value of u, $\eta \neq 0$ is a constant that controls the degree of convexity-concavity, and μ is the constant coefficient that controls the stability and the rate of convergence of the fractional-order gradient descent method. u^{v_3*} is unknown beforehand, but every iterative result is an approximate value to u^{v_3*} in the solution procedure, i.e. $u^n \to u^{v_3*}$. Thus, let $(u^n - u^{v_3*})^2 \approx \left(u^{n-1}-u^n\right)^2$, $\eta = 1$ and $\mu = 0.005$ in the following example. Thus, from (111), (112), and (113), the following can be obtained as (114)–(116), as shown at the top of this page, where we set $\prod_{\tau=1}^{n}(v_2-\tau+1)\overset{n=0}{=}1$. Secondly, the numerical implementation of the fractional-order partial differential equation should be restricted by CFL condition [122]. Thirdly, in (111) and (112), for the convenience of computation, k only takes $k = 0, 1$ as an approximation instead of $k = 0 \to \infty$. Finally, it may be considered that $u^n = 0$ and $|D^{v_1}u^n| = 0$ during the numerical iteration computation of (114) and (115). To enable (114) and (115) to be implemented, if $u^n = 0$ and $|D^{v_1}u^n| \leq \varepsilon$, let $u^n = \varepsilon$ and $|D^{v_1}u^n| = \varepsilon$, where ε is a small positive constants. Without loss of generality, in the following experiments, let $\varepsilon = 10^{-5}$.

The capability of maintaining the edges and textural details of the fractional-order denoising algorithm based on the fractional-order variational method was analyzed by considering the integer-order denoising algorithm based on the classic integer-order variational method [17]–[21] vis-à-vis the proposed fractional-order denoising algorithm and a

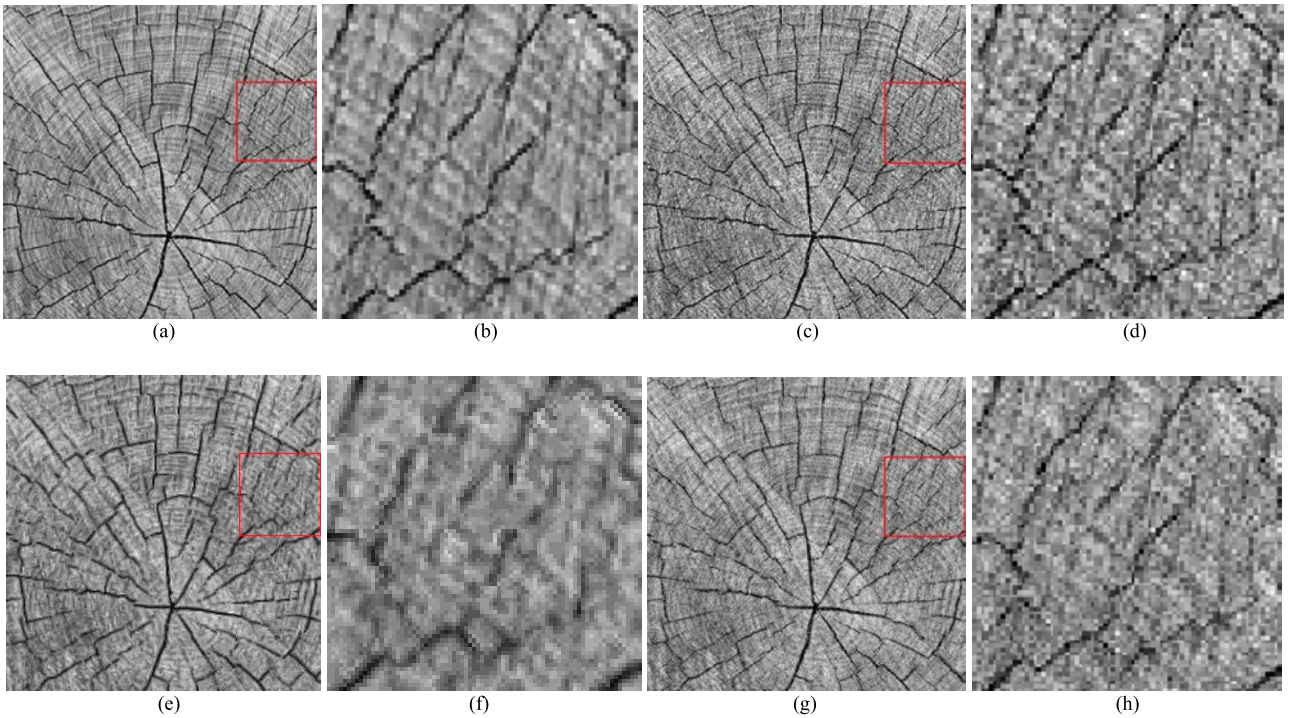

FIGURE 6. Comparative denoising experiments on a wood grain image. (a) Original wood grain image, (b) Enlarged detail of higher right 1/16 of (a), (c) Noised wood grain image, (d) Enlarged detail of higher right 1/16 of (c), (e) Integer-order denoising algorithm, (f) Enlarged detail of higher right 1/16 of (e), (g) Fractional-order denoising algorithm, (h) Enlarged detail of higher right 1/16 of (g).

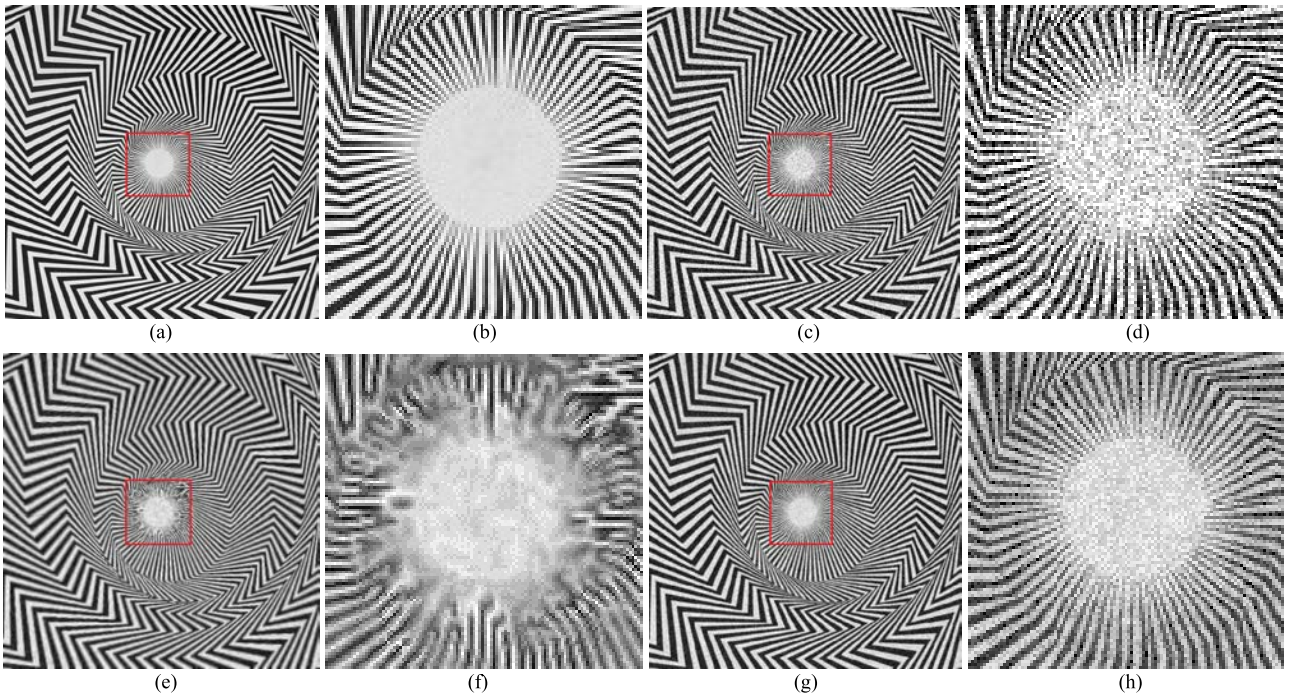

FIGURE 7. Comparative denoising experiments on a radial annulus image. (a) Original radial annulus image, (b) Enlarged detail of higher right 1/16 of (a), (c) Noised radial annulus image, (d) Enlarged detail of higher right 1/16 of (c), (e) Integer-order denoising algorithm, (f) Enlarged detail of higher right 1/16 of (e), (g) Fractional-order denoising algorithm, (h) Enlarged detail of higher right 1/16 of (g).

suitable texture image i.e. a wood grain image. Without loss of generality, let us suppose that the added noise is subject to Gaussian distribution $N(0, 10^{-2})$, with which we randomly degraded the original wood grain image and used this noised image as the test image. No *a priori* knowledge regarding the characteristics of the original wood grain image is either known or required. We set $v_1 = 1.65$, $v_2 = 2.75$, and $v_3 = 1.25$ in (114), (115), and (116). Suppose we set the same parameters, the time interval $\Delta t = 0.000625$, the number of iterations $n = 400$, for both the fractional-order denoising algorithm and the integer-order one in this simulation experiment. Thus, the results of the comparative denoising experiments for the wood grain image are shown in Fig. 6.

To consider the visual effects for the purpose of comparison, from Fig. 6 (a), (b), (e), (f), (g), and (h), we can see that the capability of the integer-order denoising algorithm based on the integer-order variational method to maintain the edges and textural details is worse than that of the fractional-order denoising algorithm based on the fractional-order variational method. In particular, the extent to which the integer-order denoising algorithm is able to maitain the local edges and textural details is relatively weaker than that of the fractional-order denoising algorithm. The integer-order denoising algorithm tends to overly smooth the noised image if there are rich high-frequency edges and textural details, often resulting in a blurry appearance of the output image. In comparison, the result of maintaining the edges and textural details of the fractional-order denoising algorithm is relatively clearer than that of the integer-order denoising algorithm. The denoised image of the integer-order denoising algorithm appears relatively smoother and more unclear than that produced by the fractional-order denoising algorithm.

Next, with the objective of performing a quantitative analysis, we obtained the PSNR between the denoised image and the original image to evaluate the denoising effects of each competing algorithm under consideration. The PSNR of the integer-order denoising algorithm and that of the fractional-order denoising algorithm are 20.2832 and 22.4786, respectively. The PSNR of the integer-order denoising algorithm is much smaller than that of the fractional-order denoising algorithm, which shows that the high-frequency edges and textural details of the denoised image of the integer-order denoising algorithm is sharply diffused and smoothed. This, in turn, indicates that the structural similarity of the edges and textural details between its corresponding denoised image and the original image is weaker than that of the fractional-order denoising algorithm. The capability of maintaining the edges and textural details of the fractional-order denoising algorithm is obviously superior to that of the integer-order denoising algorithm, especially for images rich in textural detail.

In addition, as the next experimental step, we then selected another suitable texture image i.e. a radial annulus image for the purpose of achieving comparative experiments. We also stochastically degraded the original radial annulus image with Gaussian distribution noise $N(0, 10^{-2})$ and used this noised image as the test image. No *a priori* knowledge regarding the characteristics of the original radial annulus image is either

known or required. We still set set $v_1 = 1.65$, $v_2 = 2.75$, and $v_3 = 1.25$ in (114), (115), and (116). Suppose we set the same parameters, the time interval $\Delta t = 0.000625$, the number of iterations $n = 400$, for both the fractional-order denoising algorithm and the integer-order one in this simulation experiment. Thus, the results of the comparative denoising experiments for the moonscape image are shown in Fig. 7.

From Fig. 7 (a), (b), (e), (f), (g), and (h), we can see that the result of maintaining the edges and textural details of the fractional-order denoising algorithm is relatively clearer than that of the integer-order denoising algorithm. The denoised image of the integer-order denoising algorithm appears relatively smoother than those produced by the fractional-order denoising algorithm. Next, the PSNR of the integer-order denoising algorithm and that of the fractional-order denoising algorithm are 17.1512 and 19.7222, respectively. The capability of maintaining the edges and textural details of the fractional-order denoising algorithm is obviously superior to that of the integer-order denoising algorithm, especially for images rich in textural detail.

V. CONCLUSIONS

How to apply fractional calculus to variational method is an emerging scientific field that has been seldom received desired attention. Similar to the classical first-order Euler-Lagrange equation for the first-order variational method, in fact, in fractional calculus of variations, the solutions of the fractional-order Euler-Lagrange equation are the functions for which a given fractional-order functional is stationary. In signal processing and image processing, because a differ-integrable functional is stationary at its fractional-order local maxima and minima, the fractional-order Euler-Lagrange equation is very useful for solving the fractional-order fixed boundary optimization problems in which, given some fractional-order functional, one seeks the corresponding fractional-order function minimizing (or maximizing) it. The main goal of this paper is to derive the fractional-order Euler-Lagrange equation for fractional-order variational method, which is a necessary condition for the fractional-order fixed boundary optimization problems in signal processing and image processing. Here, fractional calculus has been proposed to apply to the solution of this problem mainly because of its inherent strengths in terms of long-term memory, non-locality, and weak singularity.

In this paper, two different equivalent forms of the fractional-order Euler-Lagrange equation for the fractional-order variational method are obtained based on Wiener-Khintchine theorem and the fractional-order Green formula, respectively. At first, because the inverse Fourier transforms of $(\mathrm{j}\omega_x)^v$ and $\left(\mathrm{j}\omega_y\right)^v$ belong to Euler integral of the second kind, $\overline{D_x^v}$ and $\overline{D_y^v}$ could not be achieved in spatial domain or time domain directly, which should be implemented in discrete Fourier transform domain. Thus, the proposed fractional-order Euler-Lagrange equation based on Wiener-Khintchine theorem should be achieved by discrete Fourier transform and inverse discrete Fourier transform successively, which is difficult and complex to implement. Secondly, the proposed fractional-order Euler-Lagrange equation based on fractional-order Green formula can be directly and easily implemented in spatial domain or time domain. It is verified that the traditional first-order Euler-Lagrange equation is actually a special case of the fractional-order Euler-Lagrange equation. When we utilize the proposed fractional-order Euler-Lagrange equation based on fractional-order Green formula to deal with the classical first-order image restoration problems, it has the same results as those obtained by the classical first-order Euler-Lagrange equation. Thirdly, from the comparative experiments of image restoration such as inpainting and denoising, we can see that the capability of restoring and maintaining the edges and textural details of the fractional-order image restoration algorithm based on the fractional-order variational method is superior to that of the integer-order image restoration algorithm based on the classical first-order variational method, especially for images rich in textural details. The fractional-order Euler-Lagrange equation for the fractional-order variational method proposed by this paper is a necessary condition for the fractional-order fixed boundary optimization problems, which is a basic mathematical method in the fractional-order optimization and can be widely applied to the fractional-order field of signal analysis, signal processing, image processing, machine intelligence, automatic control, biomedical engineering, intelligent transportation, computational finance, etc..

The aforementioned discussion has also highlighted additional problems that need to be further studied. For example, further research is required to determine the image-dependent optimal values of v_1, v_2, and v_3. It will be discussed in my future work.

REFERENCES

[1] L. Euler, *Methodus Inveniendi Lineas Curvas Maximi Minimive Proprietate Gaudentes sive Solutio Problematis Isoperimetrici Latissimo Sensu Accepti*. Laussanne, Switzerland: Marc-Michel Bousquet & Compagnie, 1744.

[2] L. Euler, "Methodus inveniendi lineas curvas, additamentum I: De curvis elasticis," in *Opera Omnia Prima*, vol. 24. Bern, Switzerland: Orell Füssli, 1952, pp. 231–297.

[3] H. H. Goldstine, *A History of the Calculus of Variations From the 17th Through the 19th Century*. New York, NY, USA: Springer-Verlag, 1980.

[4] H. Erlichson, "Johann Bernoulli's brachistochrone solution using Fermat's principle of least time," *Eur. J. Phys.*, vol. 20, no. 5, pp. 299–304, 1999.

[5] C. Lanczos, *The Variational Principles of Mechanics*. New York, NY, USA: Dover Publications, 1986.

[6] D. Z. Lao, *Fundamental of the Calculus of Variations (in Chinese)*, Beijing, China: National Defense Industry Press, 2015.

[7] R. Courant, "Variational method for the solution of problems equilibrium and vibrations," *Bull. Amer. Math. Soc.*, vol. 49, pp. 1–23, Jan. 1943.

[8] M. J. Turner, R. W. Clough, H. C. Martin, and L. J. Topp, "Stiffness and deflection analysis of complex structures," *J. Aeronautical Sci.*, vol. 23, no. 9, pp. 805–823, 1956.

[9] L. E. Elsgolc, *Calculus of Variations*. London, U.K.: Pergamon Press, 1961.

[10] I. Ekeland, "Nonconvex minimization problems," *Bull. Amer. Math. Soc.*, vol. 1, no. 3, pp. 443–474, 1979.

[11] J. Hanc, S. Tuleja, and M. Hancova, "Simple derivation of newtonian mechanics from the principle of least action," *Amer. J. Phys.*, vol. 71, no. 4, pp. 386–391, 2003.

[12] S. T. Epstein, *The Variation Method in Quantum Chemistry*. New York, NY, USA: Academic Press, 1974.

[13] R. K. Nesbet, *Variational Principles and Methods in Theoretical Physics and Chemistry*. New York, NY, USA: Cambridge Univ. Press, 2003.

[14] S. K. Adhikari, *Variational Principles for the Numerical Solution of Scattering Problems*. New York, NY, USA: Wiley, 1998.

[15] S.-S. Chung and C. HsiungChen, "Partial variational principle for electromagnetic field problems: Theory and applications," *IEEE Trans. Microw. Theory Techn.*, vol. 36, no. 3, pp. 473–479, Mar. 1988.

[16] G. Leitmann, *The Calculus of Variations and Optimal Control: An Introduction*, Berlin, Germany: Springer, 1981.

[17] T. F. Chan and J. H. Shen, "A good image model eases restoration—On the contribution of Rudin–Osher–Fatmi's BV image model," IMA, Tech. Rep. 1829, Feb. 2002. [Online]. Available: https://www.researchgate.net/publication/237434927

[18] L. I. Rudin, S. Osher, and E. Fatemi, "Nonlinear total variation based noise removal algorithms," *Phys. D, Nonlinear Phenomena*, vol. 60, nos. 1–4, pp. 259–268, 1992.

[19] L. I. Rudin and S. Osher, "Total variation based image restoration with free local constraints," in *Proc. 1st IEEE Int. Conf. Image Process.*, Austin, TX, USA, Nov. 1994, pp. 31–35.

[20] T. F. Chan, S. Osher, and J. Shen, "The digital TV filter and nonlinear denoising," *IEEE Trans. Image Process.*, vol. 10, no. 2, pp. 231–241, Feb. 2001.

[21] B. Song, "Topics in variational PDE image segmentation, inpainting and denosing," Ph.D. dissertation, Univ. California Los Angeles, Los Angeles, CA, USA, 2003.

[22] S. Esedoglu and J. Shen, "Digital inpainting based on the Mumford-Shah-Euler image model," *Eur. J. Appl. Math.*, vol. 13, no. 4, pp. 353–370, 2002.

[23] J. Darbon and M. Sigelle, "Image restoration with discrete constrained total variation part I: Fast and exact optimization," *J. Math. Imag. Vis.*, vol. 26, no. 3, pp. 261–276, Dec. 2006.

[24] C. Liu, H.-Y. Shum, and W. T. Freeman, "Face hallucination: Theory and practice," *Int. J. Comput. Vis.*, vol. 75, no. 1, pp. 115–134, 2007.

[25] D. Datsenko and M. Elad, "Example-based single document image super-resolution: A global MAP approach with outlier rejection," *Multidimensional Syst. Signal Process.*, vol. 18, nos. 2–3, pp. 103–121, Sep. 2007.

[26] A. Marquina and S. J. Osher, "Image super-resolution by TV-regularization and Bregman iteration," *J. Sci. Comput.*, vol. 37, no. 3, pp. 367–382, Dec. 2008.

[27] L. H. Lieu and L. A. Vese, "Image restoration and decomposition via bounded total variation and negative Hilbert-Sobolev spaces," *Appl. Math. Optim.*, vol. 58, no. 2, pp. 167–193, Oct. 2008.

[28] S. Roth and M. J. Black, "Fields of Experts," *Int. J. Comput. Vis.*, vol. 82, no. 2, pp. 103–111, Apr. 2009.

[29] J. Dahl, P. C. Hansen, S. H. Jensen, and T. L. Jensen, "Algorithms and software for total variation image reconstruction via first-order methods," *Numer. Algorithms*, vol. 53, no. 1, pp. 67–92, Jan. 2010.

[30] K. B. Oldham, and J. Spanier, *The Fractional Calculus: Integrations and Differentiations of Arbitrary Order*. New York, NY, USA: Academic Press, 1974.

[31] A. C. McBride, *Fractional Calculus*. New York, NY, USA: Halsted Press, 1986.

[32] K. Nishimoto, *Fractional Calculus: Integrations and Differentiations of Arbitrary Order*. New Haven, CT, USA: Univ. New Haven Press, 1989.

[33] S. G. Samko, A. A. Kilbas, and O. I. Marichev, *Fractional Integrals and Derivatives: Theory and Applications*. Yverdon-les-Bains, Switzerland: Gordon and Breach Press, 1993.

[34] I. Podlubny, *Fractional Differential Equations: An Introduction to Fractional Derivatives, Fractional Differential Equations, Some Methods of Their Solution and Some of Their Applications*. San Diego, CA, USA: Academic Press, 1998.

[35] N. Özdemir and D. Karadeniz, "Fractional diffusion-wave problem in cylindrical coordinates," *Phys. Lett. A*, vol. 372, no. 38, pp. 5968–5972, Sep. 2008.

[36] N. Özdemir, O. P. Agrawal, D. Karadeniz, and B. B. Iskender, "Analysis of an axis-symmetric fractional diffusion-wave problem," *J. Phys. A, Math. Theor.*, vol. 42, no. 35, 2009, Art. no. 355208.

[37] Y. Povstenko, "Solutions to the fractional diffusion-wave equation in a wedge," *Fractional Calculus Appl. Anal.*, vol. 17, no. 1, pp. 122–135, Mar. 2014.

[38] R. C. Koeller, "Applications of fractional calculus to the theory of viscoelasticity," *J. Appl. Mech.*, vol. 51, no. 2, pp. 294–298, 1984.

[39] Y. A. Rossikhin and M. V. Shitikova, "Applications of fractional calculus to dynamic problems of linear and nonlinear hereditary mechanics of solids," *Appl. Mech. Rev.*, vol. 50, no. 1, pp. 15–67, 1997.

[40] S. Manabe, "A suggestion of fractional-order controller for flexible spacecraft attitude control," *Nonlinear Dyn.*, vol. 29, no. 1, pp. 251–268, Jul. 2002.

[41] I. Podlubny, I. Petráš, B. M. Vinagre, and P. O'Leary, and L. Dorčák, "Analogue realizations of fractional-order controllers," *Nonlinear Dyn.*, vol. 29, no. 1, pp. 281–296, Jul. s2002.

[42] Y.-F. Pu, Y. Zhang, and J.-L. Zhou, "Defense against chip cloning attacks based on fractional hopfield neural networks," *Int. J. Neural Syst.*, vol. 27, no. 1, Art. no. 1750003, p. 28, 2017. [Online]. Available: http://www.worldscientific.com/doi/abs/10.1142/S0129065717500034

[43] Y.-F. Pu, Y. Zhang, and J.-L. Zhou, "Fractional hopfield neural networks: fractional dynamic associative recurrent neural networks," *IEEE Trans. Neural Netw. Learn. Syst.*, to be published. [Online]. Available: http://ieeexplore.ieee.org/xpl/articleDetails.jsp?arnumber=7513418

[44] Y.-F. Pu, "Analog circuit realization of arbitrary-order fractional hopfield neural networks: A novel application of fractor to defense against chip cloning attacks," *IEEE Access*, vol. 4, pp. 5417–5435, 2016.

[45] Y.-F. Pu, X. Yuan, K. Liao, and J.-L. Zhou, "Implement any fractional order neural-type pulse oscillator with net-grid type analog fractance circuit," *J. Sichuan Univ. (Eng. Sci. Ed.)*, vol. 38, no. 1, pp. 128–132, 2006.

[46] C. Song and J. Cao, "Dynamics in fractional-order neural networks," *Neurocomputing*, vol. 142, pp. 494–498, Oct. 2014.

[47] E. Kaslik and S. Sivasundaram, "Dynamics of fractional-order neural networks," in *Proc. Int. Joint Conf. Neural Netw.*, San Jose, CA, USA, Aug. 2011, pp. 1375–1380.

[48] G. Carlson and C. Halijak, "Approximation of fractional capacitors (1/s)1/n by a regular Newton process," *IEEE Trans. Circuit Theory*, vol. 11, no. 2, pp. 210–213, Jun. 1964.

[49] S. D. Roy, "On the realization of a constant-argument immittance or fractional operator," *IEEE Trans. Circuit Theory*, vol. 14, no. 3, pp. 264–374, Sep. 1967.

[50] Y.-F. Pu, "Measurement units and physical dimensions of fractance-part I: Position of purely ideal Fractor in Chua's axiomatic circuit element system and fractional-order reactance of fractor in its natural implementation," *IEEE Access*, vol. 4, pp. 3379–3397, 2016.

[51] Y.-F. Pu, "Measurement units and physical dimensions of fractance-part II: Fractional-order measurement units and physical dimensions of fractance and rules for fractors in series and parallel," *IEEE Access*, vol. 4, pp. 3398–3416, 2016.

[52] Y.-F. Pu, N. Zhang, H. Wang, S.-S. Chen, X. Yuan, and L. Shu, "Order-frequency characteristics of a promising circuit element: Fractor," *J. Circuits, Syst. Comput.*, vol. 25, no. 12, 2016, Art. no. 1650156.

[53] Y.-F. Pu, X. Yuan, K. Liao, Z.-L. Chen, and J.-L. Zhou, "Five numerical algorithms of fractional calculus applied in modern signal analyzing and processing," *J. Sichuan Univ. (Eng. Sci. Ed.)*, vol. 37, no. 5, pp. 118–124, 2005.

[54] Y.-F. Pu, X. Yuan, K. Liao, J.-L. Zhou, and Y.-D. Wang, "Determination of scale sample step for getting numerical result of the continuous wavelet transform," *J. Sichuan Univ. (Eng. Sci. Ed.)*, vol. 36, no. 6, pp. 111–116, 2004.

[55] Y.-F. Pu and X. Yuan, "Fracmemristor: Fractional-order memristor," *IEEE Access*, vol. 4, pp. 1872–1888, 2016.

[56] A. Oustaloup, F. Levron, F. M. Nanot, and B. Mathieu, "Frequency-band complex noninteger differentiator: Characterization and synthesis," *IEEE Trans. Circuits Syst. I, Fundam. Theory Appl.*, vol. 47, no. 1, pp. 25–39, Jan. 2000.

[57] C.-C. Tseng, "Design of fractional order digital FIR differentiators," *IEEE Signal Process. Lett.*, vol. 8, no. 3, pp. 77–79, Mar. 2001.

[58] Y. Q. Chen and B. M. Vinagre, "A new IIR-type digital fractional order differentiator," *Signal Process.*, vol. 83, no. 11, pp. 2359–2365, Nov. 2003.

[59] A. S. Elwakil, "Fractional-order circuits and systems: An emerging interdisciplinary research area," *IEEE Circuits Syst. Mag.*, vol. 10, no. 4, pp. 40–50, 4th Quart., 2010.

[60] T. J. Freeborn, "A survey of fractional-order circuit models for biology and biomedicine," *IEEE J. Emerg. Sel. Topics Circuits Syst.*, vol. 3, no. 3, pp. 416–424, Sep. 2013.

[61] T. Tembulkar, S. Darade, S. R. Jadhav, and S. Das, "Design of fractional order differentiator & integrator circuit using RC cross ladder network," *Int. J. Emerg. Eng. Res. Technol.*, vol. 2, no. 7, pp. 127–135, Oct. 2014.

[62] Y.-F. Pu, "Research on application of fractional calculus to latest signal analysis and processing," Ph.D. dissertation, College Electron. Inf., Sichuan Univ., Chengdu, China, 2006.

[63] Y.-F. Pu, "Fractional calculus approach to texture of digital image," in *Proc. 8th IEEE Int. Conf. Signal Process.*, Beijing, China, Oct. 2006, pp. 1002–1006.

[64] Y.-F. Pu and W. X. Wang, "Fractional differential masks of digital image and their numerical implementation algorithms," *Acta Automat. Sinica*, vol. 33, no. 11, pp. 1128–1135, 2007.

[65] Y.-F. Pu, "Application of fractional differential approach to digital image processing," *J. Sichuan Univ. (Eng. Sci. Ed.)*, vol. 39, no. 3, pp. 58–78, 2007.

[66] M. Xu, J. Yang, D. Zhao, and H. Zhao, "An image-enhancement method based on variable-order fractional differential operators," *Bio-Med. Mater. Eng.*, vol. 26, no. s1, pp. S1325–S1333, 2015.

[67] D. L. Chen, C. R. Zheng, D. Y. Xue, and Y. Q. Chen, "Non-local fractional differential-based approach for image enhancement," *Res.J. Appl. Sci., Eng. Technol.*, vol. 6, no. 17, pp. 3244–3250, 2013.

[68] Y.-F. Pu, W. X. Wang, J.-L. Zhou, Y. Y. Wang, and H. D. Jia, "Fractional differential approach to detecting textural features of digital image and its fractional differential filter implementation," *Sci. China F, Inf. Sci.*, vol. 51, no. 9, pp. 1319–1339, Sep. 2008.

[69] Y.-F. Pu, J.-L. Zhou, and X. Yuan, "Fractional differential mask: A fractional differential-based approach for multiscale texture enhancement," *IEEE Trans. Image Process.*, vol. 19, no. 2, pp. 491–511, Feb. 2010.

[70] Y.-F. Pu *et al.*, "Fractional partial differential equation denoising models for texture image," *Sci. China Inf. Sci.*, vol. 57, no. 7, pp. 1–19, Jul. 2014.

[71] Y.-F. Pu, P. Siarry, J.-L. Zhou, and N. Zhang, "A fractional partial differential equation based multiscale denoising model for texture image," *Math. Methods Appl. Sci.*, vol. 37, no. 12, pp. 1784–1806, Aug. 2014.

[72] Y.-F. Pu, N. Zhang, Y. Zhang, and J.-L. Zhou, "A texture image denoising approach based on fractional developmental mathematics," *Pattern Anal. Appl.*, vol. 19, no. 2, pp. 427–445, May 2016.

[73] Y.-F. Pu, J.-L. Zhou, Y. Zhang, N. Zhang, G. Huang, and P. Siarry, "Fractional extreme value adaptive training method: Fractional steepest descent approach," *IEEE Trans. Neural Netw. Learn. Syst.*, vol. 26, no. 4, pp. 653–662, Apr. 2015.

[74] Y.-F. Pu, J.-L. Zhou, P. Siarry, N. Zhang, and Y.-G. Liu, "Fractional partial differential equation: Fractional total variation and fractional steepest descent approach based multi-scaledenoising model for texture image," *Abstract Appl. Anal.*, vol. 2013, 2013, Art. no. 483791.

[75] Y.-F. Pu and J.-L. Zhou, "A novel approach for multi-scale texture segmentation based on fractional differential," *Int. J. Comput. Math.*, vol. 88, no. 1, pp. 58–78, 2011.

[76] R. Hilfer, *Applications of Fractional Calculus in Physics*. River Edge, NJ, USA: World Scientific, 2000.

[77] M. D. Ortigueira, *Fractional Calculus for Scientists and Engineers*. Dordrecht, The Netherlands: Springer, 2011.

[78] R. Herrmann, *Fractional Calculus: An Introduction for Physicist*, River Edge, NJ, USA: World Scientific, 2011.

[79] R. Herrmann, "On the Origin of Space," *Central Eur.J. Phys.*, vol. 11, no. 10, pp. 1212–1220, 2013.

[80] R. A. El-Nabulsi, "The fractional boltzmann transport equation," *Comput. Math. Appl.*, vol. 62, no. 3, pp. 1568–1575, Aug. 2011.

[81] R. Herrmann, "Infrared spectroscopy of diatomic molecules—A fractional calculus approach," *Int. J. Modern Phys. B*, vol. 27, no. 6, 2013, Art. no. 1350019.

[82] R. Herrmann, "Gauge invariance in fractional field theories," *Phys. Lett. A*, vol. 372, no. 34, pp. 5515–5522, Aug. 2008.

[83] R. A. El-Nabulsi and G. C. Wu, "Fractional complexified field theory from saxena-kumbhat fraction integral, fractional derivative of order () and dynamical fractional integral exponent," *African Diaspora J. Math.*, vol. 13, no. 2, pp. 45–61, 2012.

[84] R. A. El-Nabulsi, "The fractional white dwarf hydrodynamical nonlinear differential equation and emergence of quark stars," *Appl. Math. Comput.*, vol. 218, no. 6, pp. 2837–2849, Nov. 2011.

[85] A. P. Riascos and J. L. Mateos, "Fractional dynamics on networks: Emergence of anomalous diffusion and Lévy flights," *Phys. Rev. E*, vol. 90, no. 3, 2014, Art. no. 032809.

[86] R. A. El-Nabulsi, "A cosmology governed by a fractional differential equation and the generalized kilbas-saigo-mittag-leffler function," *Int. J. Theor. Phys.*, vol. 55, no. 2, pp. 625–635, 2016.

[87] R. A. El-Nabulsi, "Implications of the ornstein-uhlenbeck-like fractional differential equation in cosmology," *Revista Mexicana De FÃsica*, vol. 62, no. 3, pp. 240–250, 2016.

[88] R. A. El-Nabulsi, "Fractional variational symmetries of Lagrangians, the fractional Galilean transformation and the modified Schrödinger equation," *Nonlinear Dyn.*, vol. 81, no. 1, pp. 939–948, Jul. 2015.

[89] A. Freed, K. Diethelm, and Y. Luchko, "Fractional-order viscoelasticity (FOV): Constitutive development using the fractional calculus," NASA's Glenn Research Center, Brook Park, OH, USA, Tech. Rep. NASA/TM 2002-211914, 2002.

[90] R. A. El-Nabulsi, "Fractional functional with two occurrences of integrals and asymptotic optimal change of drift in the black-scholes model," *Acta Math. Vietnamica*, vol. 40, no. 4, pp. 689–703, Dec. 2015.

[91] R. L. Magin, "Fractional Calculus in Bioengineering: Part1, Part 2 and Part 3, critical reviews in biomedical engineering," *Begell House Inc.*, vol. 32, nos. 1–4, pp. 1–378, 2004.

[92] R. A. El-Nabulsi, "The fractional kinetic einstein-vlasov system and its implications in bianchi spacetimes geometry," *Int. J. Theor. Phys.*, vol. 53, no. 8, pp. 2712–2726, Aug. 2014.

[93] G. Baumann, "Fractional calculus and symbolic solution of fractional differential equations," in *Fractals in Biology and Medicine* (Mathematics and Biosciences in Interaction). Birkhäuser Basel, Switzerland: Birkhäuser, 2005, pp. 287–298.

[94] D. Cafagna, "Fractional calculus: A mathematical tool from the past for present engineers," *IEEE Ind. Electron. Mag.*, vol. 1, no. 2, pp. 35–40, Jul. 2007.

[95] R. Marazzato and A. C. Sparavigna. (Oct. 2009). "Astronomical image processing based on fractional calculus: The AstroFracTool." [Online]. Available: https://arxiv.org/abs/0910.4637

[96] E. Ahmed and A. S. Elgazzar, "On fractional order differential equations model for nonlocal epidemics," *Phys. A, Statist. Mech. Appl.*, vol. 379, no. 2, pp. 607–614, Jun. 2007.

[97] I. Tejado, D. Valério, and N. Valério, "Fractional calculus in economic growth modelling: The spanish case," in *Proc. 11th Portuguese Conf. Autom. Control (CONTROLO)*, vol. 321. Jul. 2014, pp. 449–458.

[98] R. A. El-Nabulsi, "Fractional derivatives generalization of Einstein's field equations," *Indian J. Phys.*, vol. 87, no. 2, pp. 195–200, Feb. 2013.

[99] R. A. El-Nabulsi, "Fractional variational approach with non-standard power-law degenerate Lagrangians and a generalized derivative operator," *Tbilisi Math. J.*, vol. 9, no. 1, pp. 279–294, 2016.

[100] U. Gosh, S. Sarkar, and S. Das, "Solutions of linear fractional nonhomogeneous differential equations with jumarie fractional derivative and evaluation of particular integrals," *Amer. J. Math. Anal.*, vol. 3, no. 3, pp. 54–64, 2015.

[101] Y. Luchko and J. Trujillo, "Caputo-type modification of the Erdélyi-Kober fractional derivative," *Fractional Calculus Appl. Anal.*, vol. 10, no. 3, pp. 249–267, 2007.

[102] R. A. El-Nabulsi, "Fractional elliptic operators from a generalized Glaeske-Kilbas-Saigo-Mellin transform," *Funct. Anal., Approx. Comput.*, vol. 7, no. 1, pp. 29–33, 2015.

[103] R. A. El-Nabulsi, "The fractional calculus of variations from extended Erdélyi-Kober operator," *Int. J. Modern Phys. B*, vol. 23, no. 16, pp. 3349–3361, 2009.

[104] R. A. El-Nabulsi, "Fractional variational problems from extended exponentially fractional integral," *Appl. Math. Comput.*, vol. 217, no. 22, pp. 9492–9496, Jul. 2011.

[105] I. N. Sneddon, "The use in mathematical physics of Erdélyi-Kober operators and of some of their generalizations," in *Proc. Int. Conf. Held Univ. New Haven*, New Haven, CT, USA, Jun. 1974, pp. 37–79.

[106] R. A. El-Nabulsi and D. F. M. Torres, "Fractional action-like variational approach," *J. Math. Phys.*, vol. 49, 2008, Art. no. 053521.

[107] R. A. El-Nabulsi, "Calculus of variations with hyperdifferential operators from TabasakiŰTakebeŰToda lattice arguments," *Revista de la Real Acad. de Ciencias Exactas, Fisicas y Naturales. A, Matematicas*, vol. 107, no. 2, pp. 419–436, Sep. 2013.

[108] R. A. El-Nabulsi and D. F. M. Torres, "Necessary optimality conditions for fractional action-like integrals of variational calculus with Riemann-Liouville derivatives of order (?, ?)," *Math. Methods Appl. Sci.*, vol. 30, no. 15, pp. 1931–1939, Oct. 2007.

[109] G. Jumarie, "Modified Riemann-Liouville derivative and fractional Taylor series of nondifferentiable functions further results," *Comput. Math. Appl.*, vol. 51, nos. 9–10, pp. 1367–1376, May 2006.
[110] R. A. El-Nabulsi, "Glaeske-Kilbas-Saigo fractional integration and fractional dixmier trace," *Acta Math. Vietnamica*, vol. 37, no. 2, pp. 149–160, 2012.
[111] U. N. Katugampola, "A new approach to generalized fractional derivatives," *Bull. Math. Anal. Appl.*, vol. 6, no. 4, pp. 1–15, 2014.
[112] R. A. El-Nabulsi, "Universal fractional Euler-Lagrange equation from a generalized fractional derivate operator," *Central Eur. J. Phys.*, vol. 9, no. 1, pp. 250–256, Feb. 2011.
[113] H. M. Ozaktas, Z. Zalevsky, and M. A. Kutay, *The Fractional Fourier Transform*. Chichester, U.K.: Wiley, 2001.
[114] Y. Li, Y. Q. Chen, and I. Podlubny, "Stability of fractional-order nonlinear dynamic systems: Lyapunov direct method and generalized Mittag-Leffler stability," *Comput. Math. Appl.*, vol. 59, no. 5, pp. 1810–1821, Mar. 2010.
[115] Y. Li, Y. Q. Chen, and I. Podlubny, "Mittag–Leffler stability of fractional order nonlinear dynamic systems," *Automatica*, vol. 45, no. 8, pp. 1965–1969, Aug. 2009.
[116] W. Rudin, *Functional Analysis*. New York, NY, USA: McGraw Hill, 1991.
[117] J. Bai and X. C. Feng, "Fractional-order anisotropic diffusion for image denoising," *IEEE Trans. Image Process.*, vol. 16, no. 10, pp. 2492–2502, Oct. 2007.
[118] P. Guidotti and J. V. Lambers, "Two new nonlinear nonlocal diffusions for noise reduction," *J. Math. Imag. Vis.*, vol. 33, no. 1, pp. 25–37, Jan. 2009.
[119] J. Zhang, "Fractional-order variational PDE based image modeling and denoising algorithms," Ph.D. dissertation, Nanjing Univ. Sci. Technol., Nanjing, China, 2010.
[120] V. E. Tarasov, "Fractional vector calculus and fractional Maxwell's equations," *Ann. Phys.*, vol. 323, no. 11, pp. 2756–2778, Nov. 2008.
[121] T. J. Osler, "Leibniz rule for fractional derivatives generalized and an application to infinite series," *SIAM J. Math. Anal.*, vol. 18, no. 3, pp. 658–674, 1970.
[122] J. W. Thomas, *Numerical Partial Differential Equations: Finite Difference Methods*. New York, NY, USA: Springer-Verlag, 1995.

YI-FEI PU received the Ph.D. degree from the College of Electronics and Information Engineering, Sichuan University, in 2006.

He is a Full Professor and Doctoral Supervisor with the College of Computer Science, Sichuan University, the Chief Technology Officer of Chengdu PU Chip Science and Technology Co., Ltd., and elected into the Thousand Talents Program of Sichuan Province. His research interests include the application of fractional calculus and fractional partial differential equation to signal processing, image processing, circuits and systems, and neural networks. He has firstly authored about 20 papers indexed by SCI in journals, such as the International Journal of Neural Systems, the IEEE TRANSACTIONS ON IMAGE PROCESSING, IEEE TRANSACTIONS ON NEURAL NETWORKS AND LEARNING SYSTEMS, IEEE ACCESS, Mathematic Methods in Applied Sciences, and Science in China Series F: Information Sciences, Science China Information Sciences. He was involved in several research projects, such as the National Nature Science foundation of China and Returned Overseas Chinese Scholars Project of Education Ministry of China. He holds 12 China Inventive Patents, as the first or single inventor.